



Mussel-inspired 3D fiber scaffolds for heart-on-a-chip toxicity studies of engineered nanomaterials

Ahn, Seungkuk; Ardoña, Herdeline Ann M.; Lind, Johan U.; Eweje, Feyisayo; Kim, Sean L.; Gonzalez, Grant M.; Liu, Qihan; Zimmerman, John F.; Pyrgiotakis, Georgios; Zhang, Zhenyuan

Total number of authors:
15

Published in:
Analytical and Bioanalytical Chemistry

Link to article, DOI:
[10.1007/s00216-018-1106-7](https://doi.org/10.1007/s00216-018-1106-7)

Publication date:
2018

Document Version
Peer reviewed version

[Link back to DTU Orbit](#)

Citation (APA):

Ahn, S., Ardoña, H. A. M., Lind, J. U., Eweje, F., Kim, S. L., Gonzalez, G. M., Liu, Q., Zimmerman, J. F., Pyrgiotakis, G., Zhang, Z., Beltran-Huarac, J., Carpinone, P., Moudgil, B. M., Demokritou, P., & Parker, K. K. (2018). Mussel-inspired 3D fiber scaffolds for heart-on-a-chip toxicity studies of engineered nanomaterials. *Analytical and Bioanalytical Chemistry*, 410(24), 6141-6154. <https://doi.org/10.1007/s00216-018-1106-7>

General rights

Copyright and moral rights for the publications made accessible in the public portal are retained by the authors and/or other copyright owners and it is a condition of accessing publications that users recognise and abide by the legal requirements associated with these rights.

- Users may download and print one copy of any publication from the public portal for the purpose of private study or research.
- You may not further distribute the material or use it for any profit-making activity or commercial gain
- You may freely distribute the URL identifying the publication in the public portal

If you believe that this document breaches copyright please contact us providing details, and we will remove access to the work immediately and investigate your claim.

1 **Mussel-inspired 3D Fiber Scaffolds for Heart-on-a-Chip Toxicity Studies of Engineered**
2 **Nanomaterials**

3 Seungkuk Ahn^a, Herdeline Ann M. Ardoña^a, Johan U. Lind^{a‡}, Feyisayo Eweje^a, Sean L. Kim^a,
4 Grant M. Gonzalez^a, Qihan Liu^a, John F. Zimmerman^a, Georgios Pyrgiotakis^b, Zhenyuan Zhang^b,
5 Juan Beltran-Huarac^b, Paul Carpinone^b, Brij M. Moudgil^b, Philip Demokritou^b, and Kevin Kit
6 Parker^{*a}

7
8 ^aDisease Biophysics Group, Wyss Institute for Biologically Inspired Engineering, John A.
9 Paulson School of Engineering and Applied Sciences, Harvard University, Cambridge, MA
10 02138, USA

11 ^bCenter for Nanotechnology and Nanotoxicology, T. H. Chan School of Public Health, Harvard
12 University, Cambridge, MA 02138, USA

13 [‡]Current affiliation: Department of Micro- and Nanotechnology, Technical University of
14 Denmark, Kgs. Lyngby, Denmark

15
16

17 **KEYWORDS:** Polydopamine, Nanofiber, Microphysiological Systems, Cardiotoxicity,
18 Nanotoxicology

19

20 **Target Journal: Analytical and Bioanalytical Chemistry**

21 **Abstract word count: 248 / 250**

22

23 **Main text word count: 6,955**

24

25

26

27 ***Corresponding author:**

28 Kevin Kit Parker

29 29 Oxford St. (Rm. 321)

30 Cambridge, MA, 02138

31 Tel: (617) 495-2850

32 Fax: (617) 495-9837

33 Email: kkparker@seas.harvard.edu

34

1 Abstract

2 Due to the unique physicochemical properties exhibited by materials with nanoscale dimensions,
3 there is currently a continuous increase in the number of engineered nanomaterials (ENMs) used
4 in consumer goods. However, several reports associate ENM exposure to negative health
5 outcomes such as cardiovascular diseases. Therefore, understanding the pathological
6 consequences of ENM exposure represents an important challenge, requiring model systems that
7 can provide mechanistic insights across different levels of ENM-based toxicity. To achieve this,
8 we developed a mussel-inspired 3D microphysiological system (MPS) to measure cardiac
9 contractility in the presence of ENMs. While multiple cardiac MPS have been reported as
10 alternatives to *in vivo* testing, most systems only partially recapitulate the native extracellular
11 matrix (ECM) structure. Here, we show how adhesive and aligned polydopamine (PDA)/
12 polycaprolactone (PCL) nanofiber can be used to emulate the 3D native ECM environment of the
13 myocardium. Such nanofiber scaffolds can support the formation of anisotropic and contractile
14 muscular tissues. By integrating these fibers in a cardiac MPS, we assessed the effects of TiO₂
15 and Ag nanoparticles on the contractile function of cardiac tissues. We found that these ENMs
16 decrease the contractile function of cardiac tissues through structural damage to tissue
17 architecture. Furthermore, the MPS with embedded sensors herein presents a way to non-
18 invasively monitor the effects of ENM on cardiac tissue contractility at different time points.
19 These results demonstrate the utility of our MPS as an analytical platform for understanding the
20 functional impacts of ENMs while providing a biomimetic microenvironment to *in vitro* cardiac
21 tissue samples.

22

23

1 **Introduction**

2 Engineered nanomaterials (ENMs) have unique size-dependent optical, magnetic, and electrical,
3 properties, which can be difficult to achieve using their bulk counterparts. Consequently, the use
4 of ENMs has greatly increased in consumer products, with applications in cosmetics, electronics,
5 and even drug delivery. Because ENMs are often designed to be evenly distributed, insoluble and
6 stable, this makes them difficult to safely dispose [1] and therefore increases their potential to act
7 as environmental pollutants. This in turn, presents the risk of being exposed to ENMs via
8 unintended routes, such as through ambient air inhalation or oral ingestion via ground and
9 drinking water. As a result, understanding the pathological consequences of organ exposure to
10 ENMs poses an important challenge that has not been fully explored [2, 3]. This is particularly
11 alarming as some early reports have already linked ENM exposure with cardiac failure and
12 potentially death [4]. For instance, exposure to TiO₂ nanoparticles, which are abundantly used in
13 white pigments, sunscreens and food colorants, lead to a dose-dependent increase of heart rate
14 due to ENM-induced arrhythmia under *ex vivo* exposure conditions of guinea pig hearts [5].
15 Additionally, Ag nanoparticles, which are industrially used in mirrors, photography and as
16 antimicrobial or conducting agents, has also been found to diminish action potential readings in
17 mice and lead to loss in myocardial excitability that induces lethal bradyarrhythmia [6].
18 Collectively, this marks TiO₂ and Ag as particularly important targets, both because of their
19 deleterious role in cardiac health, but also because of their widespread manufacture and
20 distribution [7]. Although significant progress has been made in identifying the cellular impacts
21 of multiple ENMs, more investigations are needed to fully understand their mechanism of action
22 and disease pathophysiology. Among the limitations of expanding the nanotoxicological studies
23 are the high cost, low throughput, and ethical concerns of experiments involving *in vivo* and *ex*

1 *in vivo* models [8]. Accordingly, there is a great need for developing *in vitro* systems with
2 physiologically-relevant architectures and high throughputs.

3 Cardiac microphysiological systems (MPS) and heart-on-chips have been developed as *in*
4 *vitro* platforms in an effort to study the cardiopathology and cardiotoxicity [9-14]. Muscular thin
5 films (MTF), consisting of 2D anisotropic muscle tissues, have been successfully used in disease
6 modeling and drug screening in previous reports [9-19]. The microstructure of the MTF
7 platforms, built by micro-molding or micro-contact printing methods, enables the construction of
8 highly aligned and contractile laminar tissues. While MTFs replicate the essential anisotropic
9 architecture of cardiac muscle to provide physiologically-relevant functional outputs *in vitro*, it is
10 still important to recapitulate the native 3D microenvironment. Recently, nanofiber has obtained
11 a great deal of attention due to their similarity to the topographical features of natural
12 extracellular matrix (ECM) networks [20-23]. To date, synthetic nanofiber scaffolds have shown
13 promise as a means of developing *in vitro* tissue engineered 3D cardiac models [21-23].
14 Nonetheless, creating MPS that integrate nanofiber as structural cues with functional readouts
15 remains challenging. In particular, there is a need to improve the adhesion between fiber layers
16 and device parts, while simultaneously ensuring cellular adhesion and the formation of
17 functional tissues.

18 To address these challenges, we developed adhesive biohybrid nanofiber scaffolds that
19 can mimic the native cardiac ECM and can adhere to a range of MPS designs. We implement the
20 scaffolds in MPS to generate *in vitro* 3D cardiac tissue models for nanotoxicology studies, with
21 facile readouts of tissue contractility. Inspired by the ability of mussels to adhere to wet and dry
22 surfaces, we functionalized nanofiber scaffolds with chemical mimics of 3,4-
23 dihydroxyphenylalanine (DOPA)—a post-translationally modified amino acid, which serves as

1 the key adhesive component of mussel foot proteins [24, 25]. Recently, several groups have
2 developed adhesive materials based on polydopamine (PDA), which has a similar chemical
3 structure and function to DOPA [24]. PDA can be easily synthesized from dopamine (DA) via
4 catechol oxidation chemistry at alkaline conditions [26], has been applied to diverse substrates
5 (both 2D and 3D), and has been used as a substrate material for improved cell adhesion and
6 tissue development [27-30]. In this study, highly aligned polycaprolactone (PCL) nanofiber
7 doped with DA was spun using a pull spinning system with centrifugal shear force [23].
8 Subsequent to spinning, DA units incorporated within the fibers were polymerized at basic pH to
9 generate PCL/PDA nanofiber [24, 29, 31-33], which can enhance protein-coating, adhesion of
10 cells, and attachment of fiber layers to the surface of MPS devices. Here, we demonstrated the
11 ability of this nanofibrous scaffold to guide the formation of anisotropic and functional cardiac
12 tissues. Finally, we investigated the effect of direct ENM exposures on cardiac tissues using
13 fiber-coated microphysiological devices based on cantilever designs, similar to those in
14 conventional MTF assays [9-14]. We observed that exposure to a high dose of TiO₂ and to Ag
15 nanoparticles disrupted the structure and function of cardiac tissues *in vitro*. These studies
16 explored the capability of our fiber-coated MPS as a platform for conducting physiologically-
17 relevant nanotoxicology studies of 3D cardiac tissues.

18

19 **Materials and Methods**

20 **Fiber fabrication and polymerization.** Nanofibers were fabricated by using a pull spinning
21 system (see Electronic Supplementary Material Fig. S1) as described previously [23]. PCL (6%
22 wt/v, Sigma) and dopamine hydrochloride (1% wt/v, DA, Sigma-Aldrich, MO, USA) were
23 dissolved in hexafluoroisopropanol (HFIP, Oakwood Chemicals, SC, USA) and mixed overnight.

1 The polymer solution was introduced to the reservoir at a flow rate of 0.2 mL/min. The rotating
2 bristle comes in contact and elongates the polymer droplet at 30,000 RPM to form continuous
3 fibers. The spun fibers were dried for 2 h in a chemical fume hood to remove excess HFIP before
4 further characterization and measurement. After drying the fibers, they were incubated with
5 triethylammonium bicarbonate (TEAB, pH 8.5, Sigma-Aldrich, MO, USA) buffer for about 20 h
6 to initiate polymerization. After the reaction, the polymerized fibers were washed by ultrapure
7 deionized water (Invitrogen, Thermo Fischer Scientific, MA, USA) at least 3 times.

8 **Scanning electron microscopy (SEM).** The fibers were prepared on SEM stubs and sputter-
9 coated with Pt/Pd (Denton Vacuum, NJ, USA) with a thickness of 5 nm. Field emission scanning
10 electron microscopy (FESEM, Zeiss) was used to obtain SEM images of the fibers.

11 **Analysis of fiber diameter and alignment.** ImageJ software (NIH) with the DiameterJ plug-in
12 was used to determine fiber diameter and alignment from the SEM images of the fibers as
13 described in a previous study [34].

14 **Fourier transform infrared (FTIR) spectroscopy.** The FTIR spectra of the fiber scaffolds
15 were measured by using Attenuated Total Reflectance-Fourier Transform Infrared spectroscopy
16 (ATR-FTIR, Lumos, Bruker, MA, USA). As a control sample, PCL/PDA film was prepared by
17 dropping and drying a solution of PCL (6% wt/v) in HFIP doped with DA (0.2% wt/v) in TEAB
18 at room temperature. For each sample, the recorded spectrum was collected from a total of 16
19 scans and was then normalized from 0 to 1 by using OriginPro 8.6 software (Origin Lab
20 Corporation).

21 **Mechanical property testing.** Mechanical uniaxial testing followed ASTM International
22 standard C1557-14 to measure the modulus of fiber sheets. A polycarbonate sheet with a
23 thickness of 150 μm (McMaster, NJ, USA) was cut into frames with a gauge length of 5 mm to

1 match the length of the MPS cantilevers. Fiber samples were cut to 10 mm length and secured to
2 the frame using epoxy (5 Minute, Devcon, MA, USA), which was cured for 24 h. After sample
3 preparation, a frame with a sample was loaded into pneumatic grips of an Instron Model 5566
4 equipped with a 10 N Load Cell. After loading, the frame was cut to allow for pulling of the
5 sample only. For testing, 10 cycles of loading to 10% strain at 0.5 Hz, 1 Hz, 2 Hz, and 3 Hz was
6 performed to match the loading condition of the cantilever. Since there was no significant
7 difference between the measurements at different frequencies, modulus at 1 Hz were only
8 reported in the main text. The specific modulus of each sample was calculated by dividing
9 modulus (MPa) by density (g/cm^3).

10 **Qualitative adhesive property testing.** To evaluate the bioadhesive property of the fiber
11 scaffolds, we assessed the extent of fibronectin (FN, BD Biosciences, CA, USA) coating at the
12 fiber surfaces. The spun fiber scaffolds were incubated with 50 $\mu\text{g/mL}$ of FN solution in
13 deionized water for 6 h at room temperature. After which, the samples were washed with
14 deionized water 3 times and were then incubated with anti-FN antibody (rabbit, Abcam, MA,
15 USA) and a secondary antibody (goat anti-rabbit IgG (H+L) conjugated with Alexa Fluor® 546,
16 Invitrogen, Thermo Fischer Scientific, MA, USA) separately, for 1 h each. The micrographs of
17 the fluorescently stained samples were obtained using a spinning disk confocal microscope
18 (Olympus ix83, Andor spinning disk). The images were recorded on a Hamamatsu Orca Flash
19 4.0 C11440 at 16-bit depth with a 0.16 μm to 0.33 μm pixel resolution. For the statistical
20 analysis of FN absorption on the nanofiber, the fluorescent FN images on the nanofiber were
21 recorded for multiple samples ($n=3$) with multiple regions of interest (ROIs, at least 25) for each
22 condition. The coverage of FN on the nanofiber was calculated using ImageJ software and then
23 normalized to the FN coverage on PCL/DA nanofiber using OriginPro 8.6 software.

1 **Neonatal rat ventricular myocyte (NRVM) culture.** All protocols for animal experiments done
2 in this study were approved by Institutional Animal Care and Use Committee (IACUC) at
3 Harvard University. NRVMs were isolated from two-day-old Sprague–Dawley rats by following
4 previous protocols [9]. The NRVMs were cultured on the scaffolds with M199 culture media
5 supplemented with 10% heat-inactivated fetal bovine serum (FBS), 10 mM HEPES, 0.1 mM
6 MEM nonessential amino acids, 20 mM glucose, 2mM L-glutamine, 1.5 μ M vitamin B-12 and
7 50 U/mL penicillin. The FBS concentration was decreased to 2% after the first 48 h in culture. A
8 kymograph of the contraction over time was generated using ImageJ software.

9 **Immunostaining.** The cells were fixed in 4 % paraformaldehyde (PFA) and 0.05% Triton-X for
10 10 min. After fixation, the samples were incubated with a primary antibody against sarcomeric
11 α -actinin (Sigma-Aldrich, MO, USA) and 4n,6-diamidino-2-phenylindole dihydrochloride
12 (DAPI, Molecular Probes, Thermo Fischer Scientific, MA, USA) for 2 h at room temperature,
13 followed by a secondary antibody against rabbit IgG (H+L) conjugated to Alexa Fluor® 546
14 (Invitrogen, Thermo Fischer Scientific, MA, USA) for 1 h at room temperature. The samples
15 were washed by 1X phosphate buffered saline (PBS, Gibco, Thermo Fischer Scientific, MA,
16 USA) and were mounted on a glass slide with Prolong Gold anti-fade agent (Invitrogen, Thermo
17 Fischer Scientific, MA, USA). Confocal microscopy (Zeiss LSM 7 LIVE) was used to obtain
18 images of immunostained cells. 3D reconstruction of z-stacked images was performed using Zen
19 lite 2.3 software (Zeiss).

20 **Cytotoxicity measurement.** A traditional lactate dehydrogenase (LDH) assay (Promega, WI,
21 USA) was utilized to measure ENM-induced cytotoxicity for NRVMs cultured on PCL/PDA
22 nanofiber-coated MPS as described previously [35, 36]. The cell culture media from each sample
23 were collected in triplicate and then incubated with the reagents from the LDH assay kit. The

1 absorbance of the resulting solution at 490 nm was recorded using a plate reader (Synergy HT,
2 BioTek, VT, USA). Due to the considerable spectral overlap of the colorimetric components of
3 the said LDH assay with the absorption of Ag nanoparticles, the assay was not performed for the
4 samples exposed to Ag. The cytotoxic effect of Ag at the working concentration used for the
5 experiments in this study (50 $\mu\text{g/mL}$) was also assessed using an MTT (3-(4,5-dimethylthiazol-2-
6 yl)-2,5-diphenyltetrazolium bromide) assay kit (Thermo Fisher Scientific, MA, USA). The
7 background absorption from Ag nanoparticles was subtracted accordingly.

8 **Quantitative analysis of maturation of cardiomyocytes.** The maturity of cardiomyocytes
9 (sarcomere alignment, length, and packing density) on the scaffolds was evaluated by using
10 algorithms in ImageJ and MATLAB (MathWorks) as previously described [37, 38]. In these
11 algorithms, orientational order parameter (OOP) helps to quantify the sarcomeric z-line
12 formation in cardiac tissues, scaling from 0 (no alignment) to 1 (perfect alignment) based on the
13 degree of the uniaxial sarcomere components at a tissue level [37, 38]. Since the z-line
14 registration plays a crucial role in contraction of cardiac tissues, OOP can be used to explain the
15 contractile strength of the engineered cardiac tissues [37, 38].

16 **Fabrication of nanofiber-coated MPS.** Gelatin (Sigma-Aldrich, MO, USA) and microbial
17 transglutaminase (MTG, Ajinomoto, NJ, USA) were prepared with deionized water as 10% and
18 4% wt/v solutions, respectively. The gelatin solution was pre-warmed to 60 °C to homogenously
19 dissolve all powder, followed by mixing with a pre-warmed MTG solution at 37 °C. To prepare
20 the bottom substrates (see Electronic Supplementary Material Fig. S2), clean acrylic sheets (0.4
21 \times 22 \times 22 mm, Astra Products, NY, USA) were covered with a low-adhesive tape (3M, MN,
22 USA) that was pre-patterned using a laser engraving system (30 W, 24 \times 12, Epilog Laser Mini,
23 CO, USA). A selected portion was peeled and exposed to plasma treatment for 2 min (SPI

1 Plasma Prep II, PA, USA). After which, the adjacent untreated area was also peeled off. Upon
2 mixing gelatin and MTG, the resulting solution was quickly pipetted onto the exposed area. A
3 PDMS block and 200 g metal weight were sequentially placed on top of the gelatin-MTG drop to
4 have a homogenous gelatin film thickness. After curing, the PDMS was carefully lifted off the
5 gelatin surface. To these gelatin substrates, 3 mL of PCL/DA (6% wt/v / 1% wt/v) solution in
6 HFIP were spun (4 chips per run). The fiber-coated devices were incubated with TEAB buffer
7 for about 20 h at room temperature to polymerize the DA units incorporated in PCL fibers. Once
8 polymerized, the devices were washed by deionized water for at least 3 times and dried in a
9 chemical hood at room temperature. After drying the devices, each chip was engraved with the
10 layout of the cantilevers using the Epilog laser cutter system (10% speed, 3% power, and 2000
11 Hz frequency). Each fiber-coated gelatin MPS chip is comprised of 6 cantilevers (2 mm × 4 mm).
12 The samples were then re-hydrated in PBS and sterilized overnight under UV light. For seeding
13 each MPS chip with cells, 200 μL of cell suspension with a concentration of 5000 cells/μL was
14 directly pipetted onto the fiber surface. After incubating the chip with cells at 37 °C for 30 min,
15 when the cells are well adhered to the fibers, 3 mL of culture media was slowly added onto the
16 well (surface area, 9 cm²) where the MPS chip is contained.

17 **Fabrication of nanofiber-coated instrumented MPS.** Instrumented cardiac MPS were
18 fabricated as previously described with additional steps for the nanofiber layer application [14].
19 The devices were constructed layer by layer on 127.9 mm × 85.8 mm × 1.0 mm glass substrates.
20 First, silver contact pads were made along the long edges of the devices by stencil printing AG-
21 510 (Applied Ink Solutions, MA, USA) and then annealed at 190 °C for 30 min. Following this
22 step, poly(*N*-isopropylacrylamide) (PNIPAAm) release layer islands (2% wt/v in isopropanol)
23 were made using a pressure sensitive pen. Subsequently, PDMS (Sylgard 184 Dow Corning, MI,

1 USA) was applied by spin coating at 4,000 RPM for 5 min, forming a 5.2 μm thick layer.
2 Following curing overnight at 65 $^{\circ}\text{C}$, Ti-Au strain gauge wires were deposited in a two-step
3 process using two stainless steel shadow masks (NewCut, NY, USA) and an e-beam evaporator
4 (Denton, NJ, USA). A second layer of PDMS was added by spin coating at 2,000 RPM for 5 min,
5 equivalent to 11.9 μm thick layer. After curing, the devices were annealed to relieve residual
6 stress in the wires by heating at 190 $^{\circ}\text{C}$ for 30 min.

7 The nanofiber layer was applied using pull spinning as described in previous sections.
8 Prior to spinning fibers, the PDMS surface of the devices was incubated with (3-
9 aminopropyl)triethoxysilane (APTES, Sigma-Aldrich, MO, USA) overnight in an evacuated
10 desiccator. The devices were subjected to treatment with UV-ozone for 8 min preceding the
11 APTES treatment to improve aminosilane adhesion to the PDMS substrate. The devices were
12 rotated to collect fibers during spinning through attachment to a milled frame connected to a
13 DeWALT DC 720 $\frac{1}{2}$ " cordless drill driver. 10 mL of the fiber solution was loaded into a plastic
14 syringe (Becton Dickinson, NJ, USA) and flowed through polyfluroalkoxy alkane tubing (Saint-
15 Gobain, PA, USA) to a wide-point plastic needle at 0.2 mL/min by using an automated syringe
16 pump (Harvard Apparatus, MA, USA). The bristle was rotated at 30,000 RPM while the solution
17 was ejected, and the resulting fibers were collected on the device. After collection was complete,
18 the nanofiber-coated devices were incubated with TEAB buffer for polymerization.

19 Cantilevers were cut from the device using the laser cutting system described above. To
20 remove the fibers from areas of the substrate other than the cantilevers, the laser cutter was used
21 to cut circular patterns around each cantilever at the lowest possible power to avoid damage to
22 the strain gauge wires. A mask with the same pattern was cut from a sheet of low-adhesive tape
23 (3M, MN, USA), which was pressed onto the substrate and then carefully removed. This removal

1 process was repeated three times to ensure that the PDMS underneath the excess fibers was
2 completely exposed for well plate attachment. Finally, milled polycarbonate wells were attached
3 to the device by forming a thin PDMS gasket on the bottom of the well plate and joining it with
4 the now PDMS substrate using O₂ plasma treatment.

5 **Engineered nanomaterial (ENM) synthesis and physico-chemical and morphological** 6 **characterization**

7 **Citrate capped silver nanoparticles:** The Ag nanoparticles were synthesized using
8 hydrothermal method. In this method, silver salts (silver nitrate) were reduced to metallic silver
9 particles using sodium citrate at elevated temperatures [39, 40]. In a round-bottom flask
10 containing a 0.25 mM AgNO₃ solution, a sodium citrate solution (0.25 mM) was added slowly
11 with a syringe. The solution temperature was adjusted to 100 °C and the reaction carried on until
12 no more H₂ was released. The suspension was then cooled and stored. The particles were
13 characterized in terms of size, shape, purity, surface chemistry, endotoxins and biological
14 contaminants according to the protocols described by Beltran et al. [41]. The results are
15 summarized in the supplemental data (see Electronic Supplementary Material Tables S1–S3 and
16 Fig. S3).

17 **Titania:** Commercially available TiO₂ Aeroxide P25 Degussa. The particles were characterized
18 in terms of size, shape, crystallinity, density, surface area, porosity, purity, surface chemistry,
19 endotoxins and biological contaminants according to the protocols described by Beltran et al.
20 [41]. The results are summarized in the supplemental data (see Electronic Supplementary
21 Material Tables S1–S3, Figs. S4 and S5).

22 **Engineered nanomaterial (ENM) dispersion preparation.** The dispersion preparation,
23 colloidal characterization and dosimetric analysis was performed as described in great detail by

1 Deloid et al. [42-44]. The cup horn sonicator (Branson Sonifier S-450D, 400 W, with Branson 3-
2 inch cup horn) was calibrated according to the protocol by Taurozzi et al. [45] and found to
3 deliver 2.59 W/mL. A stock solution of ENMs in DNase/RNase free distilled water (Invitrogen)
4 water was prepared at a concentration of 0.5 mg/ml and was used to determine the critical
5 delivered sonication energy (DSE_{cr}). 1 ml of the stock solution was used to measure the
6 hydrodynamical diameter (dH) with DLS (Malvern Nanosizer, Worcestershire, UK). The
7 solution was sonicated for 1 min, vortexed for 30 s, and measured again. The process continued
8 until the dH and polydispersity index (PDI) were not changing significantly ($\pm 5\%$). The DSE_{cr}
9 of an ENM is defined as the DSE (in J/mL) required to achieve a solution with the lowest
10 particle agglomeration state in DI H₂O and is ENM-specific. All stock suspensions from that
11 point on were prepared according to the DSE_{cr} and were then adjusted to the desired
12 concentration. The DSE_{cr} for the TiO₂ suspensions was 380 J/mL. The 10 and 100 $\mu\text{g/mL}$ TiO₂
13 working solutions used in ENM exposure experiments were prepared by diluting the 500 $\mu\text{g/mL}$
14 stock solutions with NRVM culture medium. After 3 days of cardiac MTFs in culture, the
15 samples were exposed to a specific TiO₂ dispersion concentration for 48 h before performing the
16 optical measurements for MPS chips or devices. As our positive control for an ENM with known
17 cytotoxic effects, citrated Ag nanoparticle colloidal suspensions in cell culture media were also
18 prepared.

19 **Optical measurements and analysis for nanofiber-coated MPS.** At the time point of recording,
20 each MPS sample was transferred onto a 35 mm Petri dish with a pre-warmed Tyrode's solution
21 (1.8 mM CaCl₂, 5 mM glucose, 5 mM HEPES, 1 mM MgCl₂, 5.4 mM KCl, 135 mM NaCl, 0.33
22 mM NaH₂PO₄ at pH 7.4). The sample was washed with Tyrode's solution for at least 3 more
23 times after the transfer to remove any free-floating nanoparticles and their aggregates. The

1 cantilevers were carefully peeled off the acrylic sheet while the dish is on a heating block (37 °C)
2 under a Leica MZ9.5 stereomicroscope (Wetzlar, Germany) with 1.25X magnification. **The**
3 **macroscopic motions of the cantilever, such as bending or tissue contraction,** were optically
4 recorded for each chip for at least 5 s at 30 frames per second using a Basler A601f-2 camera
5 (Exton, PA, USA), under spontaneous or paced conditions. The pacing was executed at 1, 2, and
6 3 Hz at 10 V using a MyoPacer Cell Stimulator (IonOptix, MA, USA). The changes in tissue
7 contractile stresses upon ENM exposure were determined in correspondence with our previous
8 work on MTFs cantilevers. Previously, we have demonstrated that the contractile stress of soft
9 tissues on cantilever supports, can be obtained by tracking the x-projection a cantilever's edge to
10 calculate curvature, and use a modified Stoney's equation to obtain stress [11, 12, 15]. Similar to
11 these previous reports, we assumed that the radius of curvature (R_{curv}) upon cantilever bending
12 should be directly proportional to the contractile stress of the seeded cardiomyocyte layer (σ_{tissue})
13 [11, 12]. From the generated $1/R_{\text{curv}}$ plot over time from the optical recordings, we compared the
14 extracted values proportional to σ_{tissue} across different ENM exposure conditions and performed
15 statistical analysis. All ENMs were added in the culture media at Day 3, which is 24 h after the
16 cells are supplemented by a 2% FBS culture medium. Samples that showed no contraction prior
17 to the addition of ENMs, assumedly from poor tissue maturation, were excluded from the study.
18 Spontaneous and stimulated contraction were then recorded on Day 5, for both controls and
19 samples containing ENMs. For the samples that did not show contractions at Day 5 (48 h after
20 ENM exposure), the x-projection at all recorded frames is equal to the maximum length of the
21 cantilever, therefore, yielding a value of 0 for the $1/R_{\text{curv}}$ as the calculated R_{curv} converges to
22 infinity.

1 **Data acquisition from nanofiber-coated instrumented MPS.** Data was acquired using a
2 custom polycarbonate connector and a Keithley Multichannel DMM 3706a. The 2-wire
3 resistance recordings were collected at a sampling rate of 60 Hz. A mechanical model based on a
4 modified Stoney's equation was applied to convert to resistance readout to approximate the
5 contractile stresses generated by the tissues, as previously described [14]. Custom MATLAB
6 (MathWorks) scripts were used for quantifying relative resistance changes and converting to
7 stress. For electrically paced samples, a median filter (5) was applied.

8 **Calcium imaging.** The calcium transients of cardiomyocyte samples were measured using a
9 calcium sensitive dye as described previously [46]. 50 μg of Fluo-4 AM dye (Thermo Fisher
10 Scientific, MA, USA) was prepared in Pluronic F-127 solution (20% in dimethyl sulfoxide,
11 DMSO) at 37 °C. From this stock solution, 2 μL of the dye in DMSO was added to 2 mL of
12 NRVM cell culture media with 2% FBS in 37 °C, where cardiomyocytes were incubated for 30
13 min. After incubation, the samples were washed with fresh 2% FBS media for 15 min. Then, the
14 samples were moved to a 35 mm Petri dish with 4 mL of pre-warmed Tyrode's solution in 37 °C
15 for imaging. Confocal microscopy (Zeiss LSM 7 LIVE) was used to obtain time-series images of
16 the dye from the samples.

17 **Statistical analysis.** All data are shown as mean \pm standard error of mean (SEM). One-way
18 analysis of variance (ANOVA) was utilized to determine statistical significance ($*p < 0.10$ or **
19 $p < 0.05$).

20

21 **Results and Discussion**

22 **Fabrication and characterization of mussel-inspired adhesive nanofiber**

1 Mussel-inspired adhesive nanofiber was produced by spinning precursor nanofiber and
2 polymerizing the spun nanofiber via catechol oxidation chemistry occurring under alkaline
3 conditions (Fig. 1a). The precursor nanofiber was fabricated by co-spinning PCL and DA in
4 HFIP using a pull spinning system (Fig. 1b and [see Electronic Supplementary Material Fig. S1](#))
5 [23]. Due to the low molecular weight of DA, PCL was used as a carrier polymer to form hybrid
6 nanofiber under shear forces generated in the system. Following previous reports [24, 29, 31-33,
7 47], the spun PCL/DA nanofiber was polymerized by incubating them in TEAB buffer whose pH
8 (8.5) triggers oxidization and polymerization of the accessible monomer DA units incorporated
9 in the PCL fibers (Fig. 1c). Although the structure of PDA remains poorly explored [47], herein
10 we used the term PDA as defined in the references. We chose to co-spin PCL and DA and do
11 post-polymerization instead of surface coating PCL fibers with PDA, because the latter surface
12 treatment causes non-homogeneous coating and potentially alters the nanofiber morphology [29,
13 48]. After initiating the polymerization, a color change was observed from white (PCL/DA) to
14 deep brown (PCL/PDA) fibers (insets in Figs. 1b and 1c), which is consistent with previously
15 reported PDA substrates [24, 31-33]. Fiber diameters of precursor and polymerized nanofiber
16 were 579 ± 123 nm and 591 ± 143 nm (Fig. 1d), respectively, showing no significant difference
17 in the fiber diameter before and after polymerization. Fiber alignment analysis (Fig. 1e) indicated
18 that PCL/DA and PCL/PDA nanofiber were highly aligned because of circumferentially directed
19 forces during fiber formation as previously described [23].

20 Beyond the observed color change in Figs. 1b and 1c, FT-IR spectra of the nanofiber
21 were recorded to confirm the presence of newly formed bonds after the TEAB buffer treatment
22 and to validate the occurrence of polymerization (Fig. 2a). The emergence of new IR bands near
23 1596 cm^{-1} (for C=C) and near 3200 cm^{-1} (for secondary amines, N-H) [49], after the alkaline

1 treatment of PCL/DA nanofiber, are indicative that DA cyclization has occurred to form PDA
2 units (Fig. 1a). It should nonetheless be noted that we did not quantify the extent of DA
3 polymerization and the amount of PDA that remain integrated within the fiber construct after the
4 reaction. We also investigated the mechanical strength of the nanofiber scaffolds as this plays a
5 crucial role in the optimal functionality of these fibers as tissue scaffolds. The specific modulus
6 of PCL/DA and PCL/PDA nanofiber scaffolds were calculated as $98.0 \pm 38.5 \text{ MPa}/(\text{g}\cdot\text{cm}^{-3})$ and
7 $81.4 \pm 16.7 \text{ MPa}/(\text{g}\cdot\text{cm}^{-3})$, respectively (Fig. 2b). There was no significant difference in the
8 specific modulus before and after polymerization, which suggests that the TEAB treatment
9 mostly yielded surface polymerization of DA to PDA. To assess the adhesive properties of the
10 nanofiber, we evaluated the adhesion of an ECM protein (fibronectin, FN) by immunostaining
11 (Figs. 2c-2h). Fibronectin is one of the primary ECM proteins that control cell adhesion,
12 proliferation, and functional tissue formation. After 6 h incubation at room temperature, FN
13 coverage on the surface of PCL/PDA nanofiber was higher than that on the surface of PCL/DA
14 nanofiber (Fig. 2i). This observation is in line with previous studies showing higher protein and
15 cell adhesion on PDA-coated PCL nanofiber compared to PCL nanofiber [28, 48].

16

17 ***In vitro* cardiomyocyte culture on nanofiber**

18 We hypothesized that the ECM-mimetic and adhesive properties of the nanofiber scaffold will
19 support cardiomyocyte adhesion and functional tissue formation. To test the hypothesis, we
20 cultured neonatal rat ventricular myocytes (NRVMs) on the scaffold. After a week of cell culture,
21 contractile tissues were developed on the fibrous scaffold (Figs. 3a, 3b, 3c, and see Electronic
22 Supplementary Material Fig. S6). Kymograph of the contraction (Fig. 3d and see Electronic

1 **Supplementary Material** Movie 1) reflects the regular and spontaneous beating of
2 cardiomyocytes on the scaffold at a physiological range [50].

3 In an effort to further study the maturity of cardiomyocytes, we performed
4 immunostaining for sarcomeric α -actinin and analyzed parameters related to sarcomere structure
5 [37, 38]. First, the orientational order parameter (OOP) is a metric to evaluate anisotropy of
6 elements, where 0 and 1 mean no alignment and perfect alignment, respectively [37, 38]. From
7 the cardiomyocytes seeded on our scaffolds, we observed anisotropic tissue formation along the
8 long axis of the fiber direction (Fig. 3e). The sarcomeric OOP value for these cardiomyocytes
9 grown on the mussel-inspired fiber scaffolds was 0.78 ± 0.04 , showing very high tissue
10 anisotropy. We also quantified the sarcomere length (SL) and sarcomere packing density (SPD)
11 for our tissue samples to account for the existence of fully formed sarcomeres. The cardiac
12 tissues on the scaffold exhibited $1.91 \pm 0.08 \mu\text{m}$ (for SL) and 0.18 ± 0.09 (for SPD). The OOP,
13 SL, and SPD values from the tissues on PCL/PDA nanofiber were similar to those previously
14 reported [37, 38] from the anisotropic and contractile tissue grown on 2D micro-patterned
15 substrates. Consequently, these data support our hypothesis that PCL/PDA nanofiber promotes
16 3D functional cardiac tissue formation (see **Electronic Supplementary Material** Fig. S6).

17

18 **Fiber-coated cardiac microphysiological devices for nanotoxicology studies**

19 To obtain functional data of contractile performance of the cardiac tissues, we integrated the
20 mussel-inspired nanofiber scaffolds into an MPS design based on gelatin cantilever substrates
21 [12]. By tracking the deflection of the cantilevers, we obtained *in vitro* readouts of contractile
22 function of engineered cardiac tissues cultured in physiologically-relevant 3D environments (Fig.
23 4a, see **Electronic Supplementary Material** Fig. S6, and Movie 2). We used $1/R_{\text{curv}}$ (Fig. 4b),

1 which is directly proportional to the tissue contractile stress (σ_{tissue}), as a geometrical metric to
2 assess the toxic effects of ENM exposure to cardiac tissues. This parameter is independent of any
3 assumptions regarding the multilayer nature of the substrate. We therefore performed our
4 nanotoxicological studies by comparing quantifiable geometric changes (i.e., $1/R_{\text{curv}}$) in the
5 cantilever pre- and post-ENM exposure. By plotting $1/R_{\text{curv}}$ over time, we were able to
6 extrapolate an analytical metric from the optical recordings that reflects the systolic and diastolic
7 phases of contraction of the cardiomyocyte tissue layer (Figs. 4c-d). With the assumption that
8 $1/R_{\text{curv}}$ is directly proportional to contractile tissue stress (σ_{tissue}) [11, 12, 15], normalizing the
9 peak-to-peak amplitude of the $1/R_{\text{curv}}$ plots with respect to the measurements for the control
10 samples (i.e., no ENM exposure) on the same day enables a relative comparison of the twitch
11 stress across the cardiac MPS samples under different exposure conditions.

12 With the considerations for analysis discussed above, we assessed the tissue-level effects
13 of ENM exposure at a low (10 $\mu\text{g/mL}$) and high (100 $\mu\text{g/mL}$) TiO_2 dose for NRVM tissues
14 cultured on fiber-coated gelatin MPS samples. These concentrations were selected based on the
15 range used in literature precedents that report cellular-level effects of TiO_2 to cardiac cells. A
16 previous report on the cellular toxicity of TiO_2 nanoparticles on human embryonic stem-cell
17 derived cardiomyocytes showed that 10 $\mu\text{g/mL}$ TiO_2 has no significant cytotoxic effects, while a
18 reduction in contraction amplitude was observed at 100 $\mu\text{g/mL}$ [51]. This dose-dependent
19 decrease in cell survival, as well as increase in reactive oxygen species (ROS) production, was
20 also observed for rat cardiac (H9c2) cells directly exposed to 5 to 100 $\mu\text{g/mL}$ of TiO_2 P25
21 Degussa nanoparticles [52]. Moreover, a typical nanoparticle used as a therapeutic drug
22 transporter would be delivered at a concentration of 50 $\mu\text{g}/20\text{ g}$ body weight, corresponding to

1 37 $\mu\text{g/mL}$ [51, 53]. This concentration is within the range of test concentrations used in these
2 studies (10-100 $\mu\text{g/mL}$).

3 The mechanism of action of TiO_2 toxicity is limited to general cellular-level information
4 such as ROS generation, DNA peroxidation, or directly binding to lactate dehydrogenase (LDH)
5 [54-56]. In rats, TiO_2 nanoparticles are reported to acutely alter cardiac excitability leading to
6 arrhythmogenesis [57]. In a zebrafish model, chronic TiO_2 exposure resulted in alterations in
7 cardiac muscle fibers, tissue-level inflammation and cell necrosis [58]. While the exact
8 mechanisms of the cardiotoxic effects of TiO_2 on mammalian species are less understood, silver
9 nanoparticles are well-known to induce cytotoxic effects by enhancing ROS generation that leads
10 to oxidative stress and inflammatory effects [59, 60]. Hence, we used Ag nanoparticles as a
11 positive control ENM with pronounced cardiotoxicity.

12 We evaluated the effect of Ag and TiO_2 ENM on the contractile stress generated by the
13 cardiac tissues on fiber-coated MPS, both spontaneously and under electrical pacing. In both
14 cases, we observed a dose dependent response where the samples exposed to 100 $\mu\text{g/mL}$
15 concentration of TiO_2 showed lower contractile stresses than those exposed to 10 $\mu\text{g/mL}$ and
16 unexposed conditions (Figs. 4e and 4f). As a comparison, the observed maximum $1/R_{\text{curv}}$ and
17 normalized twitch stress for samples with high dose TiO_2 exposure was still higher than those
18 exposed to the known cytotoxic Ag nanoparticles. For each condition (see Electronic
19 Supplementary Material Table S4), we also calculated for the percentage of cantilevers beating at
20 the time point of optical recording. Among the cantilevers exposed to 100 $\mu\text{g/mL}$ TiO_2 and 50
21 $\mu\text{g/mL}$ Ag, only 56% and 29% remained beating, respectively. For the other two conditions, 95%
22 of the unexposed control and 92% of the 10 $\mu\text{g/mL}$ TiO_2 -exposed cantilevers remained beating
23 across all the MPS samples at the time point of optical measurements. These results further

1 support the observable impairment in contractile function due to the exposure of cardiac tissue
2 samples to 100 $\mu\text{g/mL}$ TiO_2 and 50 $\mu\text{g/mL}$ Ag for 48 h.

3 Considering that our PDA-functionalized nanofibrous scaffolds potentially bind well to a
4 range of materials, we took advantage of this adhesive property to integrate the fiber-supported
5 cardiac tissues into instrumented MPS devices based on PDMS cantilevers with embedded
6 flexible electronic contractility sensors (Fig. 5a and [see Electronic Supplementary Material](#)
7 Movie 3). We recently reported this concept using MTFs developed on molded PDMS surfaces
8 as cardiac tissue models [13, 14]. Furthermore, we previously demonstrated potential
9 applications of the sensors for higher-throughput drug screening and time-resolved studies [13,
10 14]. Here, we show that it is straightforward to replace the molded PDMS surfaces with
11 nanofibrous scaffolds, by coating the surface of the device with adhesive PCL/PDA nanofiber
12 (Fig. 5a). This fiber-coated version combines a physiologically-relevant 3D tissue
13 microenvironment, with embedded sensors for non-invasive monitoring of tissue contractile
14 stress. Taking advantage of the embedded sensors, we performed a proof-of-principle toxicity
15 study of 100 $\mu\text{g/mL}$ TiO_2 nanoparticles, monitoring contractile stress at multiple time points for
16 the same cantilever. Again, we observed a relative decrease in the measurable twitch stress from
17 spontaneously contracting cardiac microtissues after 48 h of exposure to 100 $\mu\text{g/mL}$ TiO_2 as
18 compared to the timepoint prior to ENM exposure (Fig. 5b). Additionally, we performed a proof-
19 of-principle time-resolved study of tissue response to 100 $\mu\text{g/mL}$ TiO_2 , using the integrated
20 electrical sensors. This indicated that the spontaneous contractions became negligible after
21 merely 24 h of exposure (Fig. 5c).

22 To confirm the findings from our MPS-based studies on the influence of ENMs on
23 cardiac tissue contractile function, we performed a colorimetric assay for lactate dehydrogenase

1 (LDH), a marker for tissue necrosis [61]. This allowed us to assess the impact of ENM exposure
2 at the cellular level. Our results showed increased LDH levels upon exposure to 100 $\mu\text{g/mL}$ TiO_2
3 as compared to the control and 10 $\mu\text{g/mL}$ TiO_2 exposure (see Electronic Supplementary Material
4 Fig. S7a). We also validated the cytotoxic effect of the Ag nanoparticle dose (50 $\mu\text{g/mL}$) used in
5 these studies using an MTT assay (see Electronic Supplementary Material Fig. S7b) [62],
6 whereby 48 h of NRVM exposure to Ag led to an 86% decrease in cellular viability.

7 We also investigated the electrophysiological effect of the nanoparticles using a calcium-
8 sensitive dye (Figs. 6a–f) [46]. The fluorescent intensity of the dye during spontaneous
9 contraction of cardiomyocytes was recorded using confocal microscopy and plotted. Calcium
10 imaging showed that cardiomyocytes in the control sample contracted synchronously (Figs. 6a
11 and 6b, and see Electronic Supplementary Material Movie 4). After directly exposing the cardiac
12 tissues in MPS samples to 10 $\mu\text{g/mL}$ TiO_2 (Figs. 6c and 6d, and see Electronic Supplementary
13 Material Movie 5), a synchronized contraction of cardiomyocytes was also observed. However,
14 the higher TiO_2 dose (100 $\mu\text{g/mL}$) caused a non-synchronous calcium transient (Figs. 6e and 6f,
15 and see Electronic Supplementary Material Movie 6) in line with the decreased contractility
16 recorded using our MPS-based contractility assay (Figs. 4 and 5). The cardiac MPS samples
17 exposed to cytotoxic Ag nanoparticles (50 $\mu\text{g/mL}$), as our positive control, consistently resulted
18 in an impaired calcium transient propagation (see Electronic Supplementary Material Figs. S8a
19 and S8b).

20 From our findings, we hypothesize that the higher dose exposure of TiO_2 nanoparticles
21 can disrupt the sarcomere architecture, which correlates to the decreased contractile function
22 observed in the cardiac MPS. To test this premise, we performed structural analysis of our
23 cardiac tissue samples by immunostaining against sarcomeric α -actinin. Cardiomyocytes,

1 without the nanoparticle exposure, formed an anisotropic tissue along the alignment of the
2 nanofiber layers and revealed a perpendicular z-line registration (Fig. 6g) that plays a vital role in
3 effective pump function. Cardiomyocytes with a low dose of TiO₂ nanoparticles still showed a
4 similar organization of z-lines (Fig. 6h). However, the exposure to a high dose of TiO₂ or silver
5 nanoparticles caused disruption of the sarcomeric z-line architecture (Fig. 6i and **see Electronic**
6 **Supplementary Material Fig. S8c**). In order to quantify the sarcomere architecture, the OOP of
7 sarcomeres at different ENM exposure conditions were calculated (Fig. 6j). There was no
8 significant difference between control and low dose TiO₂ (10 µg/mL) exposure samples.
9 However, the OOP value of high dose TiO₂ (100 µg/mL) exposure samples were significantly
10 decreased with respect to the non-exposed control.

11 **Even though we showed promising results using the fibrous MPS for screening the**
12 **toxicity of ENMs, it should be noted that there are still some technical limitations for these**
13 **current devices. This system only includes one cell type (cardiomyocytes) as a proof-of-concept.**
14 **However, heart or other organs are composed of multiple cells types and interconnected to other**
15 **organs to function efficiently at the macroscopic level. To address this issue, future studies may**
16 **include multi-cellular MPS to represent the complexity of native organs. Likewise, our systems**
17 **can be integrated with multiple organs in one MPS to predict the toxicological impacts of ENMs**
18 **by considering organ cross-talk and different ENM biodistribution routes. Beyond contractility,**
19 **chronic “on-chip” measurement of action potentials using a high-throughput instrumented device**
20 **with 3D scaffolds such as this would also be beneficial for future toxicology studies.**

21 Altogether, our data demonstrated that the low dose exposure of TiO₂ nanoparticles (10
22 µg/mL) does not significantly affect the structure and function of *in vitro* cardiomyocyte tissue
23 samples within the time range of our ENM exposure studies. However, the high dose exposure of

1 TiO₂ nanoparticles (100 µg/mL) demonstrated impaired contractile function and damaged tissue
2 structure after only 48 h of exposure. The dose-dependent cardiac effects of TiO₂ nanoparticles is
3 in accord with previously published work [51]. In addition to previously reported tissue damage,
4 we also observed a decrease in sarcomere organization and interruptions in the propagation of
5 calcium signaling, suggesting an underlying cause for functional tissue damage. This shows that
6 the measurements of contractile function derived from the fiber-coated MPS presented herein,
7 provided consistent insights with conventional cytotoxic and structural analyses of tissue
8 impairment due to ENM exposure. Overall, these consistent observations validate the capability
9 of our 3D fiber-coated MPS to be used as an *in vitro* analytical platform to assess the
10 toxicological effects of ENMs to cardiac function at multiple time points.

11

12 **Conclusions**

13 In this study, we present a biomimetic platform that can be used as an *in vitro* analytical assay to
14 determine the effects of different nanoparticles on cardiac tissue contractility. The engineered
15 mussel-inspired nanofiber, which is comprised of PCL and PDA units, resulted in highly aligned
16 constructs that provided a topographical cue for the consistent formation of anisotropic cardiac
17 tissues across multiple samples. Moreover, the nanofiber facilitated cellular adhesion and ECM
18 protein coating due to their bioadhesive property. Cardiomyocytes grown on the nanofiber
19 scaffolds developed into mature and functional tissues, as confirmed by previously reported
20 metrics. Finally, the fiber-coated cardiac microphysiological devices were developed and
21 cultured with cardiomyocytes for the contractility assay and toxicity studies. The effects of direct
22 ENM exposure were tested using our MPS device platform, which provided insights and
23 established trends in the measured contractile behavior of cardiac tissues at different exposure

1 conditions that were consistent with the disruption of normal sarcomere alignment in tissues and
2 calcium signaling observed using conventional assays. In principle, the instrumented version of
3 our 3D fiber-coated MPS enables a non-invasive method towards higher-throughput
4 toxicological studies. Therefore, these findings demonstrate the capability of our 3D nanofibrous
5 MPS platform to not only recapitulate the 3D native structure of the myocardium *in vitro*, but
6 also to serve as a reliable platform to study the cardiotoxic effects of engineered nanomaterials.

7

8

9 **Acknowledgements**

10 This work was supported by the Wyss Institute for Biologically Inspired Engineering at Harvard
11 University. For the development and characterization of 3D nanofibrous MPS platform, this
12 research was performed in part at the Harvard University Materials Research Science and
13 Engineering Center (MRSEC) under NSF Award No. DMR-1420570 and the Harvard Center for
14 Nanoscale Systems (CNS), which is a member of the National Nanotechnology Infrastructure
15 Network (NNIN) under NSF Award No. 1541959. Research reported in this publication was
16 supported by National Institute of Environmental Health Sciences of the National Institutes of
17 Health under Award Number (NIH grant number U01ES027272) as part of the Nanotechnology
18 Health Implications Research (NHIR) Consortium. The content is solely the responsibility of the
19 authors and does not necessarily represent the official views of the National Institutes of Health.
20 The engineered nanomaterials used in the research presented in this publication have been
21 procured or synthesized and characterized by the Engineered Nanomaterials Resource and
22 Coordination Core (ERCC) at the Center for Nanotechnology and Nanotoxicology at Harvard

1 School of Public Health, part of the NIEHS/NHIR consortium. The authors also acknowledge the
2 graphic works provided by Michael Rosnach.

3

4 **Compliance with Ethical Standards**

5 **Disclosure of potential conflicts of interest.** The authors declare that they have no conflict of
6 interest.

7

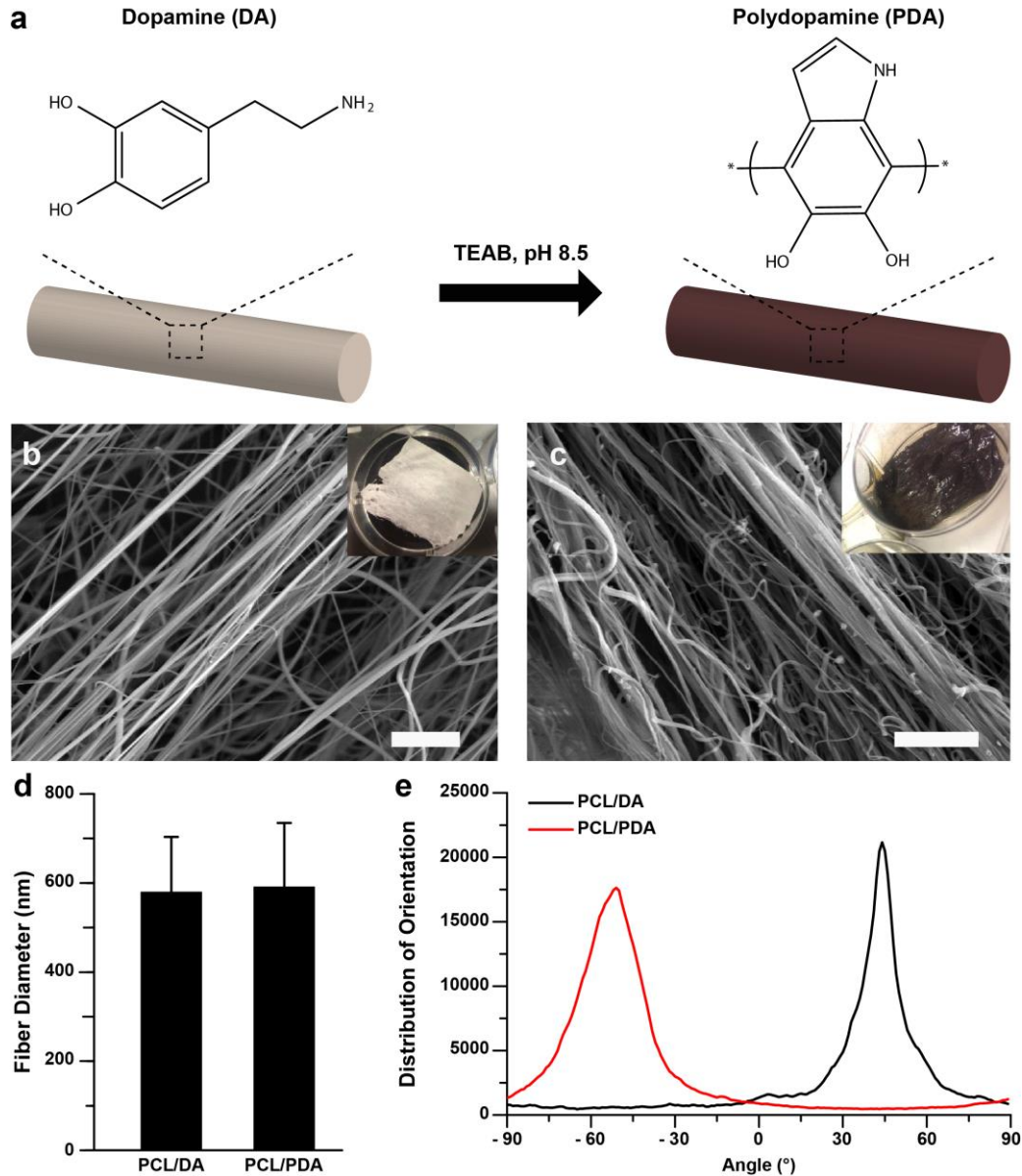
8 **References**

- 9 1. Walser T, Limbach LK, Brogioli R, Erismann E, Flamigni L, Hattendorf B et al. Persistence
10 of engineered nanoparticles in a municipal solid-waste incineration plant. *Nat Nanotechnol.*
11 2012;7(8):520.
- 12 2. Simeonova PP, Erdely A. Engineered nanoparticle respiratory exposure and potential risks for
13 cardiovascular toxicity: predictive tests and biomarkers. *Inhalation Toxicol.* 2009;21(sup1):68-73.
- 14 3. Yokel RA, MacPhail RC. Engineered nanomaterials: exposures, hazards, and risk prevention.
15 *J Occup Med Toxicol.* 2011;6(1):7.
- 16 4. Gwinn MR, Vallyathan V. Nanoparticles: health effects—pros and cons. *Environ Health*
17 *Perspect.* 2006;114(12):1818.
- 18 5. Stampfl A, Maier M, Radykewicz R, Reitmeir P, Göttlicher M, Niessner R. Langendorff heart:
19 a model system to study cardiovascular effects of engineered nanoparticles. *ACS nano.*
20 2011;5(7):5345-53.
- 21 6. Lin C-X, Yang S-Y, Gu J-L, Meng J, Xu H-Y, Cao J-M. The acute toxic effects of silver
22 nanoparticles on myocardial transmembrane potential, I Na and I K1 channels and heart rhythm
23 in mice. *Nanotoxicology.* 2017;11(6):827-37.
- 24 7. Mueller NC, Nowack B. Exposure modeling of engineered nanoparticles in the environment.
25 *Environ Sci Technol.* 2008;42(12):4447-53.
- 26 8. Sun H, Xia M, Austin CP, Huang R. Paradigm shift in toxicity testing and modeling. *AAPS J.*
27 2012;14(3):473-80.
- 28 9. Grosberg A, Alford PW, McCain ML, Parker KK. Ensembles of engineered cardiac tissues for
29 physiological and pharmacological study: heart on a chip. *Lab Chip.* 2011;11(24):4165-73.
- 30 10. Grosberg A, Nesmith AP, Goss JA, Brigham MD, McCain ML, Parker KK. Muscle on a chip:
31 in vitro contractility assays for smooth and striated muscle. *J Pharmacol Toxicol Methods.*
32 2012;65(3):126-35.
- 33 11. Shim J, Grosberg A, Nawroth JC, Parker KK, Bertoldi K. Modeling of cardiac muscle thin
34 films: pre-stretch, passive and active behavior. *J Biomech.* 2012;45(5):832-41.
- 35 12. McCain ML, Agarwal A, Nesmith HW, Nesmith AP, Parker KK. Micromolded gelatin
36 hydrogels for extended culture of engineered cardiac tissues. *Biomaterials.* 2014;35(21):5462-71.

- 1 13. Lind JU, Busbee TA, Valentine AD, Pasqualini FS, Yuan H, Yadid M et al. Instrumented
2 cardiac microphysiological devices via multimaterial three-dimensional printing. *Nat Mater.*
3 2016.
- 4 14. Lind JU, Yadid M, Perkins I, O'Connor BB, Eweje F, Chantre CO et al. Cardiac
5 microphysiological devices with flexible thin-film sensors for higher-throughput drug screening.
6 *Lab Chip.* 2017;17(21):3692-703.
- 7 15. Feinberg AW, Feigel A, Shevkoplyas SS, Sheehy S, Whitesides GM, Parker KK. Muscular
8 thin films for building actuators and powering devices. *Science.* 2007;317(5843):1366-70.
- 9 16. Agarwal A, Goss JA, Cho A, McCain ML, Parker KK. Microfluidic heart on a chip for
10 higher throughput pharmacological studies. *Lab Chip.* 2013;13(18):3599-608.
- 11 17. McCain ML, Sheehy SP, Grosberg A, Goss JA, Parker KK. Recapitulating maladaptive,
12 multiscale remodeling of failing myocardium on a chip. *Proc Natl Acad Sci.* 2013;110(24):9770-
13 5.
- 14 18. Nesmith AP, Agarwal A, McCain ML, Parker KK. Human airway musculature on a chip: an
15 in vitro model of allergic asthmatic bronchoconstriction and bronchodilation. *Lab Chip.*
16 2014;14(20):3925-36.
- 17 19. Wang G, McCain ML, Yang L, He A, Pasqualini FS, Agarwal A et al. Modeling the
18 mitochondrial cardiomyopathy of Barth syndrome with induced pluripotent stem cell and heart-
19 on-chip technologies. *Nat Med.* 2014;20(6):616.
- 20 20. Pham QP, Sharma U, Mikos AG. Electrospinning of polymeric nanofibers for tissue
21 engineering applications: a review. *Tissue Eng.* 2006;12(5):1197-211.
- 22 21. Badrossamay MR, McIlwee HA, Goss JA, Parker KK. Nanofiber assembly by rotary jet-
23 spinning. *Nano Lett.* 2010;10(6):2257-61.
- 24 22. Badrossamay MR, Balachandran K, Capulli AK, Golecki HM, Agarwal A, Goss JA et al.
25 Engineering hybrid polymer-protein super-aligned nanofibers via rotary jet spinning.
26 *Biomaterials.* 2014;35(10):3188-97.
- 27 23. Deravi LF, Sinatra NR, Chantre CO, Nesmith AP, Yuan H, Deravi SK et al. Design and
28 Fabrication of Fibrous Nanomaterials Using Pull Spinning. *Macromol Mater Eng.* 2017;302(3).
- 29 24. Liu Y, Ai K, Lu L. Polydopamine and its derivative materials: synthesis and promising
30 applications in energy, environmental, and biomedical fields. *Chem Rev.* 2014;114(9):5057-115.
- 31 25. Lin Q, Gourdon D, Sun C, Holten-Andersen N, Anderson TH, Waite JH et al. Adhesion
32 mechanisms of the mussel foot proteins mfp-1 and mfp-3. *Proc Natl Acad Sci.*
33 2007;104(10):3782-6.
- 34 26. Lee H, Rho J, Messersmith PB. Facile conjugation of biomolecules onto surfaces via mussel
35 adhesive protein inspired coatings. *Adv Mater.* 2009;21(4):431-4.
- 36 27. Chuah YJ, Koh YT, Lim K, Menon NV, Wu Y, Kang Y. Simple surface engineering of
37 polydimethylsiloxane with polydopamine for stabilized mesenchymal stem cell adhesion and
38 multipotency. *Sci Rep.* 2015;5.
- 39 28. Ku SH, Park CB. Human endothelial cell growth on mussel-inspired nanofiber scaffold for
40 vascular tissue engineering. *Biomaterials.* 2010;31(36):9431-7.
- 41 29. Dhand C, Barathi VA, Ong ST, Venkatesh M, Harini S, Dwivedi N et al. Latent Oxidative
42 Polymerization of Catecholamines as Potential Cross-linkers for Biocompatible and
43 Multifunctional Biopolymer Scaffolds. *ACS Appl Mater Interfaces.* 2016;8(47):32266-81.
- 44 30. Choi W, Lee S, Kim SH, Jang JH. Polydopamine Inter-Fiber Networks: New Strategy for
45 Producing Rigid, Sticky, 3D Fluffy Electrospun Fibrous Polycaprolactone Sponges. *Macromol*
46 *Biosci.* 2016;16(6):824-35.

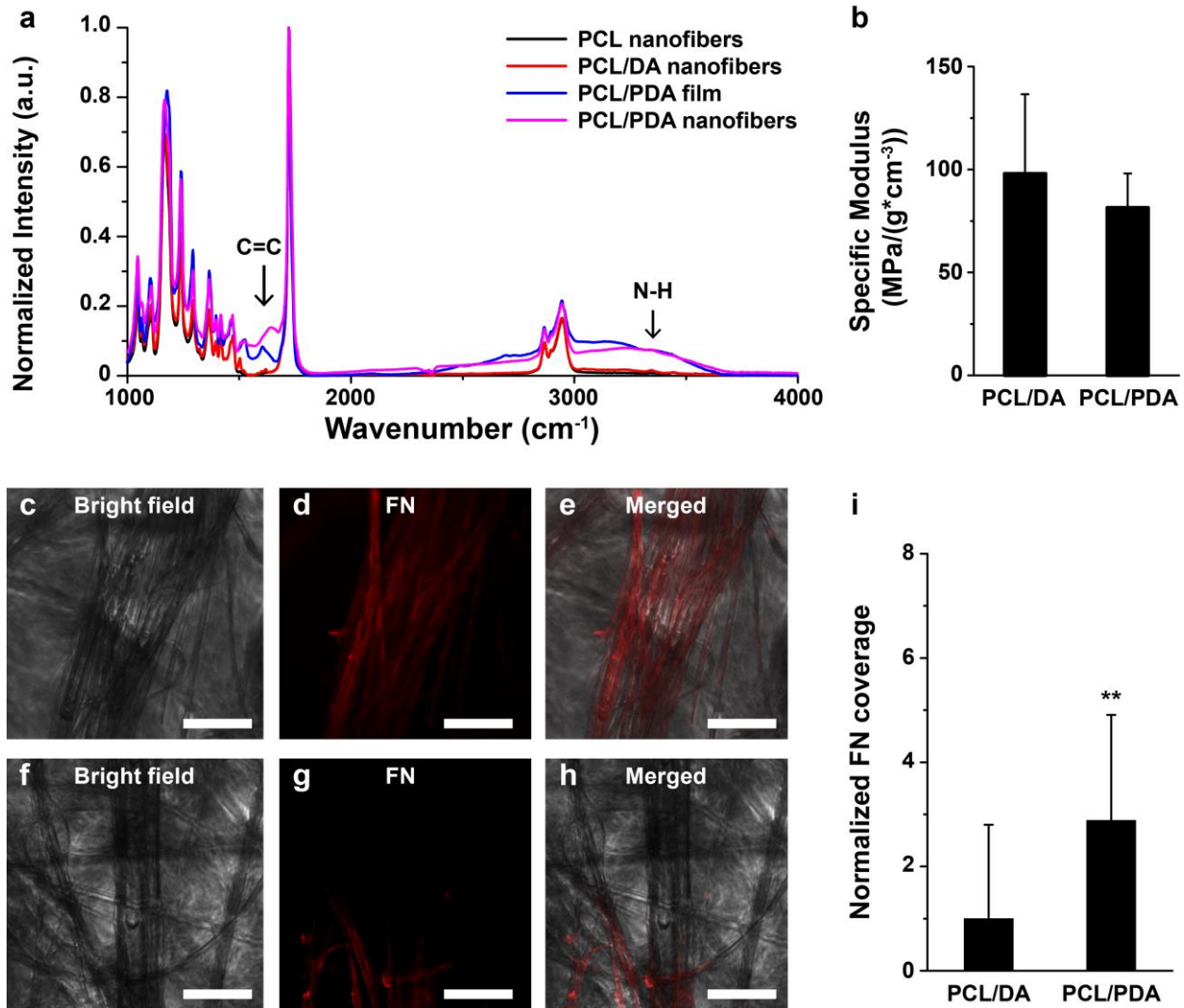
- 1 31. Della Vecchia NF, Luchini A, Napolitano A, D'Errico G, Vitiello G, Szekely N et al. Tris
2 buffer modulates polydopamine growth, aggregation, and paramagnetic properties. *Langmuir*.
3 2014;30(32):9811-8.
- 4 32. Klosterman L, Ahmad Z, Viswanathan V, Bettinger CJ. Synthesis and Measurement of
5 Cohesive Mechanics in Polydopamine Nanomembranes. *Adv Mater Interfaces*. 2017;4(10).
- 6 33. Patel K, Singh N, Yadav J, Nayak JM, Sahoo SK, Lata J et al. Polydopamine films changes
7 their physiochemical and antimicrobial properties with change in reaction conditions. *Phys Chem*
8 *Chem Phys*. 2018.
- 9 34. Hotaling NA, Bharti K, Kriel H, Simon CG. DiameterJ: A validated open source nanofiber
10 diameter measurement tool. *Biomaterials*. 2015;61:327-38.
- 11 35. Chan FK-M, Moriwaki K, De Rosa MJ. Detection of necrosis by release of lactate
12 dehydrogenase activity. *Immune Homeostasis*. Springer; 2013. p. 65-70.
- 13 36. Ahn S, Chantre CO, Gannon AR, Lind JU, Campbell PH, Grevesse T et al. Soy
14 protein/cellulose nanofiber scaffolds mimicking skin extracellular matrix for enhanced wound
15 healing. *Adv Healthcare Mater*. 2018.
- 16 37. Sheehy SP, Pasqualini F, Grosberg A, Park SJ, Aratyn-Schaus Y, Parker KK. Quality metrics
17 for stem cell-derived cardiac myocytes. *Stem Cell Rep*. 2014;2(3):282-94.
- 18 38. Pasqualini FS, Sheehy SP, Agarwal A, Aratyn-Schaus Y, Parker KK. Structural phenotyping
19 of stem cell-derived cardiomyocytes. *Stem Cell Rep*. 2015;4(3):340-7.
- 20 39. Tran QH, Le A-T. Silver nanoparticles: synthesis, properties, toxicology, applications and
21 perspectives. *Adv Nat Sci: Nanosci Nanotechnol*. 2013;4(3):033001.
- 22 40. Lee KJ, Jun BH, Kim TH, Joung J. Direct synthesis and inkjetting of silver nanocrystals
23 toward printed electronics. *Nanotechnology*. 2006;17(9):2424.
- 24 41. Beltran-Huarac J, Zhang Z, Pyrgiotakis G, DeLoid G, Vaze N, Demokritou P. Development
25 of reference metal and metal oxide engineered nanomaterials for nanotoxicology research using
26 high throughput and precision flame spray synthesis approaches. *NanoImpact*. 2018;10:26-37.
- 27 42. DeLoid GM, Cohen JM, Pyrgiotakis G, Demokritou P. Preparation, characterization, and in
28 vitro dosimetry of dispersed, engineered nanomaterials. *Nat Protoc*. 2017;12(2):355.
- 29 43. DeLoid GM, Cohen JM, Pyrgiotakis G, Pirela SV, Pal A, Liu J et al. Advanced
30 computational modeling for in vitro nanomaterial dosimetry. *Part Fibre Toxicol*. 2015;12(1):32.
- 31 44. DeLoid G, Cohen JM, Darrah T, Derk R, Rojanasakul L, Pyrgiotakis G et al. Estimating the
32 effective density of engineered nanomaterials for in vitro dosimetry. *Nat Commun*. 2014;5:3514.
- 33 45. Taurozzi JS, Hackley VA, Wiesner MR. Ultrasonic dispersion of nanoparticles for
34 environmental, health and safety assessment—issues and recommendations. *Nanotoxicology*.
35 2011;5(4):711-29.
- 36 46. Dvir T, Timko BP, Brigham MD, Naik SR, Karajanagi SS, Levy O et al. Nanowired three-
37 dimensional cardiac patches. *Nat Nanotechnol*. 2011;6(11):720.
- 38 47. Liescher Jr, Mrówczyński R, Scheidt HA, Filip C, Hädade ND, Turcu R et al. Structure of
39 polydopamine: a never-ending story? *Langmuir*. 2013;29(33):10539-48.
- 40 48. Xie J, Michael PL, Zhong S, Ma B, MacEwan MR, Lim CT. Mussel inspired protein-
41 mediated surface modification to electrospun fibers and their potential biomedical applications. *J*
42 *Biomed Mater Res, Part A*. 2012;100(4):929-38.
- 43 49. Zangmeister RA, Morris TA, Tarlov MJ. Characterization of polydopamine thin films
44 deposited at short times by autoxidation of dopamine. *Langmuir*. 2013;29(27):8619-28.

- 1 50. Boudreau-Béland J, Duverger JE, Petitjean E, Maguy A, Ledoux J, Comtois P.
2 Spatiotemporal stability of neonatal rat cardiomyocyte monolayers spontaneous activity is
3 dependent on the culture substrate. *PLoS One*. 2015;10(6):e0127977.
- 4 51. Jawad H, Boccaccini AR, Ali NN, Harding SE. Assessment of cellular toxicity of TiO₂
5 nanoparticles for cardiac tissue engineering applications. *Nanotoxicology*. 2011;5(3):372-80.
- 6 52. Mallik A, Bryan S, Puukila S, Chen A, Khaper N. Efficacy of Pt-modified TiO₂
7 nanoparticles in cardiac cells. *Exp Clin Cardiol*. 2011;16(1):6.
- 8 53. Schwerdt A, Zintchenko A, Concia M, Roesen N, Fisher K, Lindner LH et al. Hyperthermia-
9 induced targeting of thermosensitive gene carriers to tumors. *Hum Gene Ther*.
10 2008;19(11):1283-92.
- 11 54. Bostan HB, Rezaee R, Valokala MG, Tsarouhas K, Golokhvast K, Tsatsakis AM et al.
12 Cardiotoxicity of nano-particles. *Life Sci*. 2016;165:91-9.
- 13 55. Duan Y, Liu H, Zhao J, Liu C, Li Z, Yan J et al. The effects of nano-anatase TiO₂ on the
14 activation of lactate dehydrogenase from rat heart. *Biol Trace Elem Res*. 2009;130(2):162-71.
- 15 56. Sheng L, Wang X, Sang X, Ze Y, Zhao X, Liu D et al. Cardiac oxidative damage in mice
16 following exposure to nanoparticulate titanium dioxide. *J Biomed Mater Res, Part A*.
17 2013;101(11):3238-46.
- 18 57. Savi M, Rossi S, Bocchi L, Gennaccaro L, Cacciani F, Perotti A et al. Titanium dioxide
19 nanoparticles promote arrhythmias via a direct interaction with rat cardiac tissue. *Part Fibre*
20 *Toxicol*. 2014;11(1):63.
- 21 58. Chen J, Dong X, Xin Y, Zhao M. Effects of titanium dioxide nano-particles on growth and
22 some histological parameters of zebrafish (*Danio rerio*) after a long-term exposure. *Aquat*
23 *Toxicol*. 2011;101(3-4):493-9.
- 24 59. Carlson C, Hussain SM, Schrand AM, K. Braydich-Stolle L, Hess KL, Jones RL et al.
25 Unique cellular interaction of silver nanoparticles: size-dependent generation of reactive oxygen
26 species. *J Phys Chem B*. 2008;112(43):13608-19.
- 27 60. AshaRani P, Low Kah Mun G, Hande MP, Valiyaveetil S. Cytotoxicity and genotoxicity of
28 silver nanoparticles in human cells. *ACS nano*. 2008;3(2):279-90.
- 29 61. Han X, Gelein R, Corson N, Wade-Mercer P, Jiang J, Biswas P et al. Validation of an LDH
30 assay for assessing nanoparticle toxicity. *Toxicology*. 2011;287(1-3):99-104.
- 31 62. Altunbek M, Culha M. Influence of Plasmonic Nanoparticles on the Performance of
32 Colorimetric Cell Viability Assays. *Plasmonics*. 2017;12(6):1749-60.

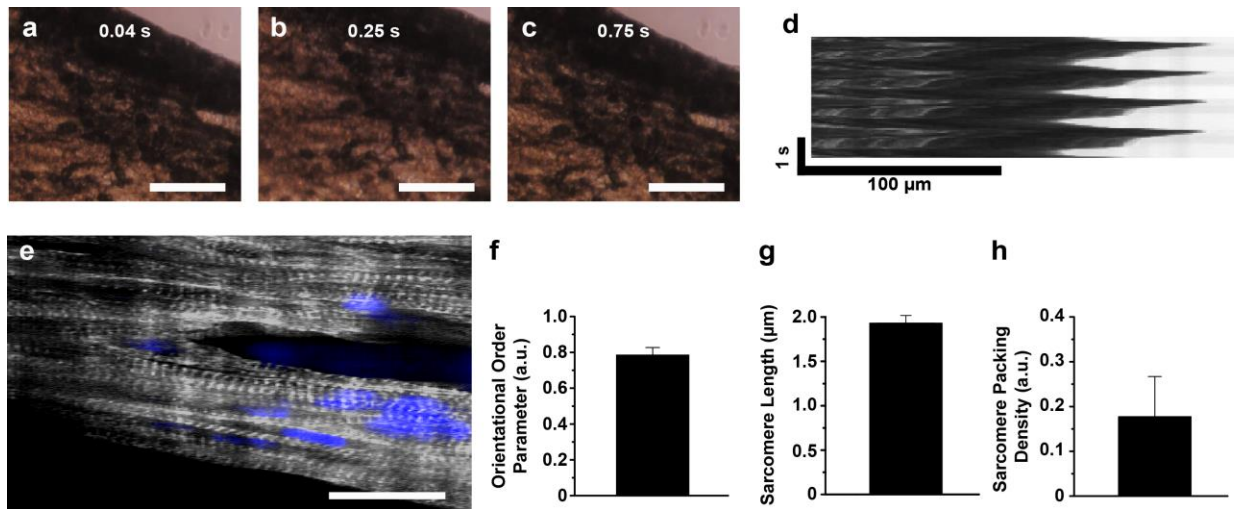


1

2 **Figure 1.** Nanofiber fabrication. (a) Schematic illustration of polymerization of PCL/DA into
 3 PCL/PDA through treatment with triethylammonium bicarbonate (TEAB, pH 8.5) buffer. (b–c)
 4 SEM images of b) PCL/DA and c) PCL/PDA. Insets indicate macroscopic images of nanofibers.
 5 Scales are 10 μm . d) Fiber diameter analysis. $n=4$. e) Fiber directionality calculated from (b–c)
 6 SEM images.

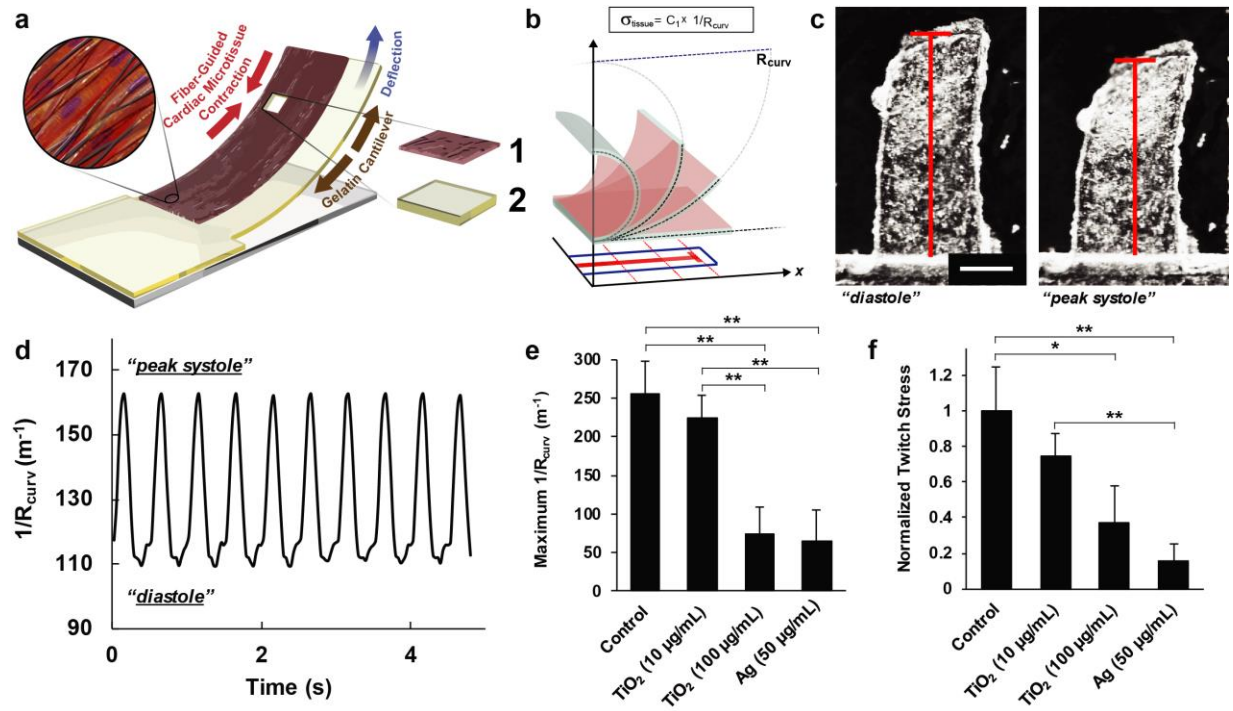


1
2 **Figure 2.** Physicochemical properties of nanofiber. a) FT-IR spectrum of PCL nanofiber,
3 PCL/DA nanofiber, PCL/PDA film, and PCL/PDA nanofiber. b) Specific modulus of nanofiber
4 scaffolds. $n=4$ for PCL/DA and $n=5$ for PCL/PDA. c–i) Adhesion of fibronectin on (c–e)
5 PCL/PDA and (f–h) PCL/DA nanofiber. Scales are 100 μm . (i) FN coverages on the nanofiber
6 were calculated and plotted. $**p<0.05$, $n=3$, ROI = at least 25 for each condition.
7
8
9
10
11

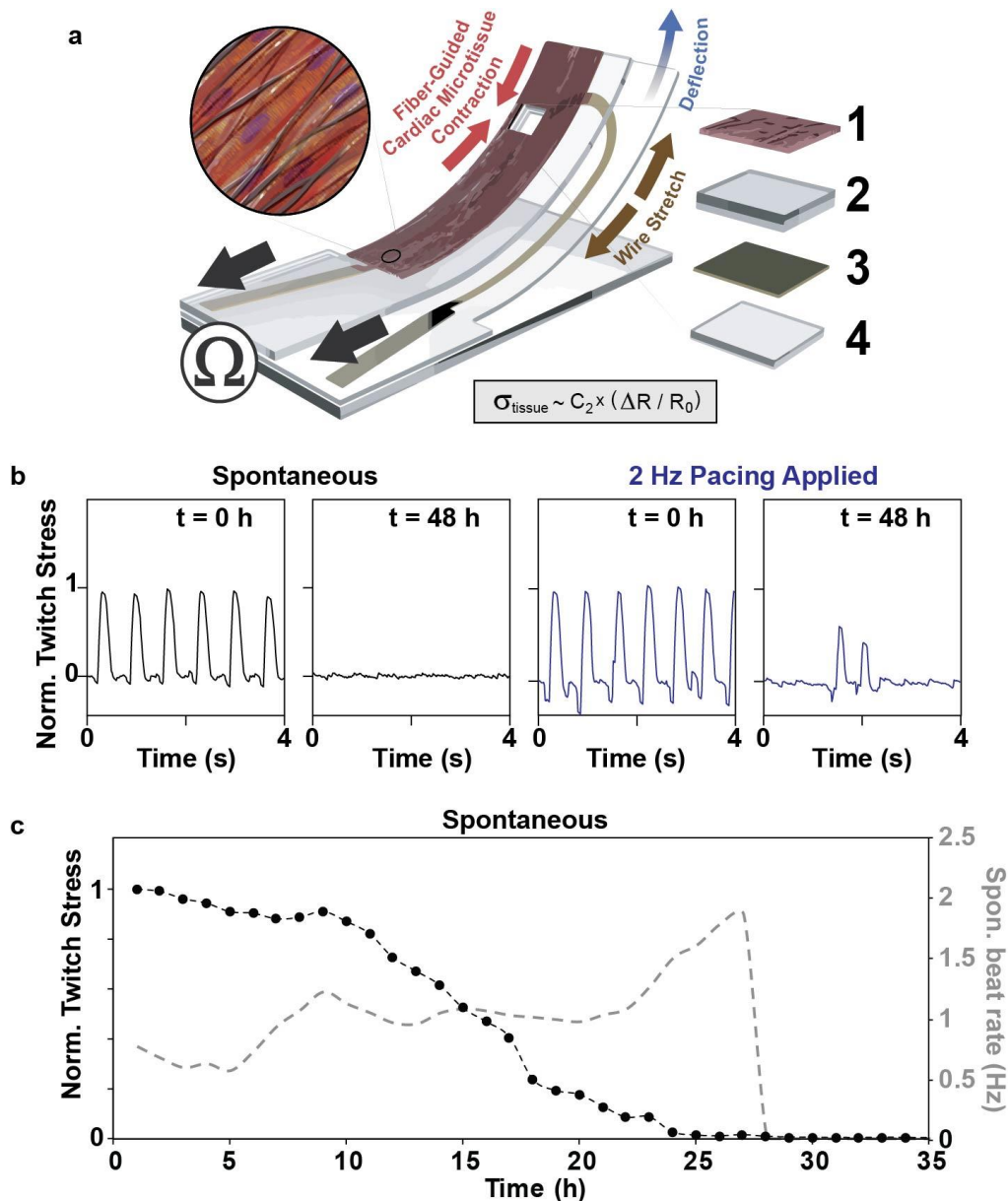


1
2 **Figure 3.** *In vitro* cardiomyocyte culture on nanofiber. a–d) (a–c) Bright field images of
3 contraction of the fiber scaffolds with (d) kymograph. Scales of a–c are 100 μm . e) Confocal
4 image of cardiomyocytes on nanofiber, stained for nuclei (blue) and α -actinin (grey). Scale is 20
5 μm . f–h) (f) Orientational order parameter (OOP), g) sarcomere length, and h) sarcomere
6 packing density (SPD) of cardiomyocytes grown on the fibrous scaffolds. $n=3$ and ROI=4.

7
8
9
10
11
12
13
14
15
16
17
18
19
20
21
22
23
24
25
26
27
28
29
30
31
32
33



1
2 **Figure 4.** Measuring contractile stress using fiber-coated gelatin MPS. a) Principle sketch of a
3 fiber-coated MPS with cardiomyocytes. Constituent layer 1: engineered cardiac tissue within
4 nanofiber scaffolds and 2: gelatin thin film; see Electronic Supplementary Material Movie 2 for a
5 representative video of a fiber-coated gelatin MPS seeded with contracting NRVMs. b)
6 Schematic diagram showing the extrapolation of x-projections of cantilever deflection in 2D and
7 its correlation to R_{curv} . c) Optical images showing the cantilever motions associated to
8 cardiomyocyte diastole and systole. Scale is 1 mm. d) Representative plot of the geometric
9 readout from the optical recording of MPS motion over time, under 2 Hz pacing. e–f)
10 Comparison of (e) maximum $1/R_{\text{curv}}$ and (f) normalized twitch stress values calculated from Day
11 5 cardiac MPS samples under different ENM exposure conditions (48 h after ENM addition, 2
12 Hz pacing at 10 V), For statistical comparison, $*p < 0.10$ and $**p < 0.05$, $n = 10$ for control, $n = 6$ for
13 10 and 100 $\mu\text{g/ml}$ and TiO_2 , and $n = 7$ for Ag (50 $\mu\text{g/ml}$).
14
15
16
17
18
19
20
21
22
23
24
25
26
27
28



1
 2 **Figure 5.** Fiber-coated cardiac microphysiological device with embedded contractility sensors. a)
 3 Principle sketch of device: an embedded flexible thin film sensor provides non-invasive
 4 electrical readout of contractile stress generated by PCL/PDA nanofiber-supported cardiac
 5 micro-tissue. Device adapted from Ref. [14] by introducing PCL/PDA nanofiber coating onto
 6 device surface. Constituent layer 1: engineered cardiac tissue within nanofiber scaffolds, 2:
 7 PDMS layer, 3: thin film sensor layer, and 4: bottom PDMS layer; see Electronic Supplementary
 8 Material Movie 3 for a representative video of a fiber-coated device seeded with contracting
 9 NRVMs. b) Electrical readout of normalized twitch stress generated by tissue prior to and after
 10 48 hrs of exposure to (100 $\mu\text{g}/\text{ml}$) TiO_2 . c) Electrical readout of normalized twitch stress (black
 11 traces, left axis) and beat rate (mean (3) grey trace, right axis) generated spontaneously by tissue
 12 during first 35 h of exposure to (100 $\mu\text{g}/\text{ml}$) TiO_2 .

13
 14

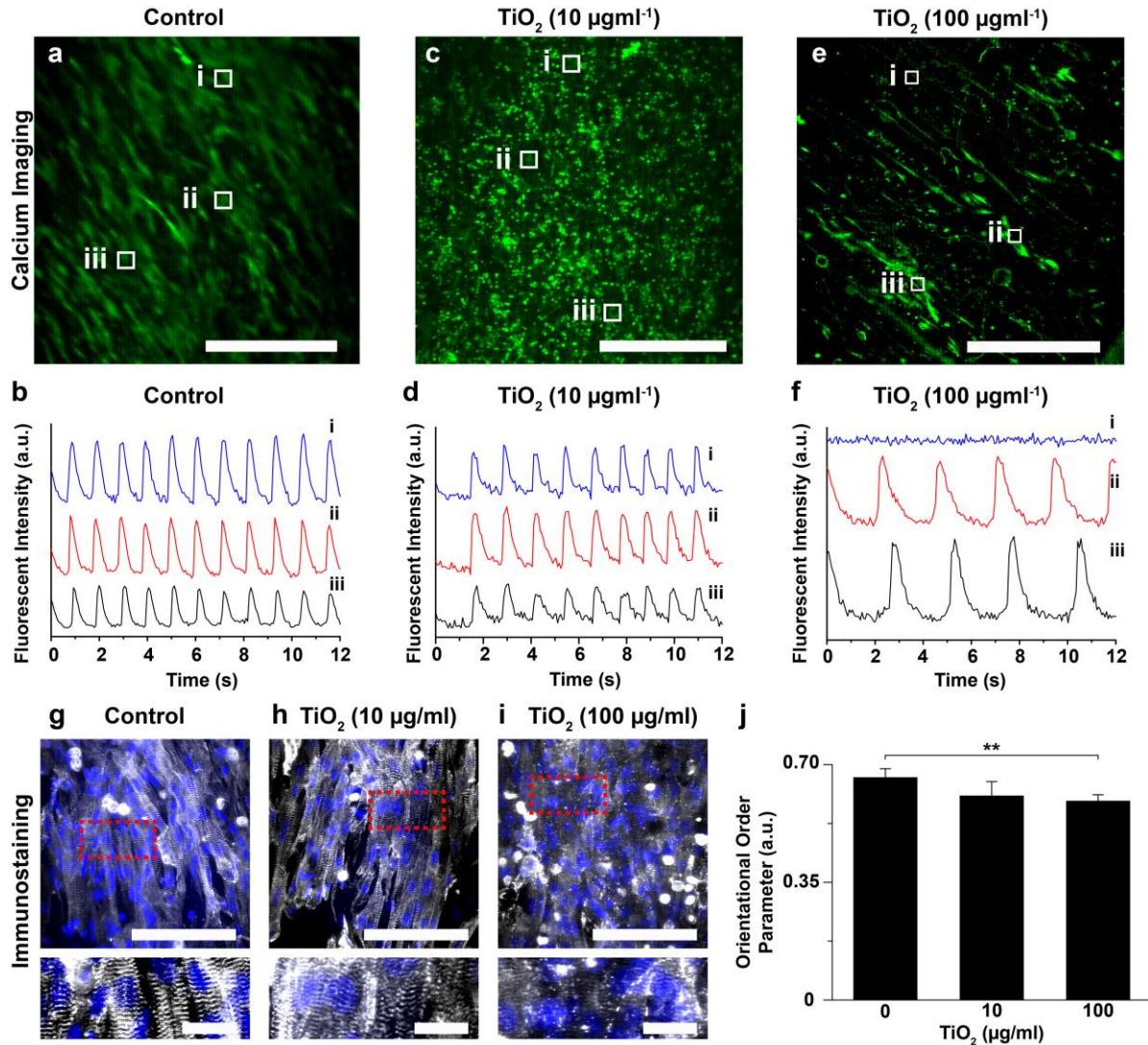
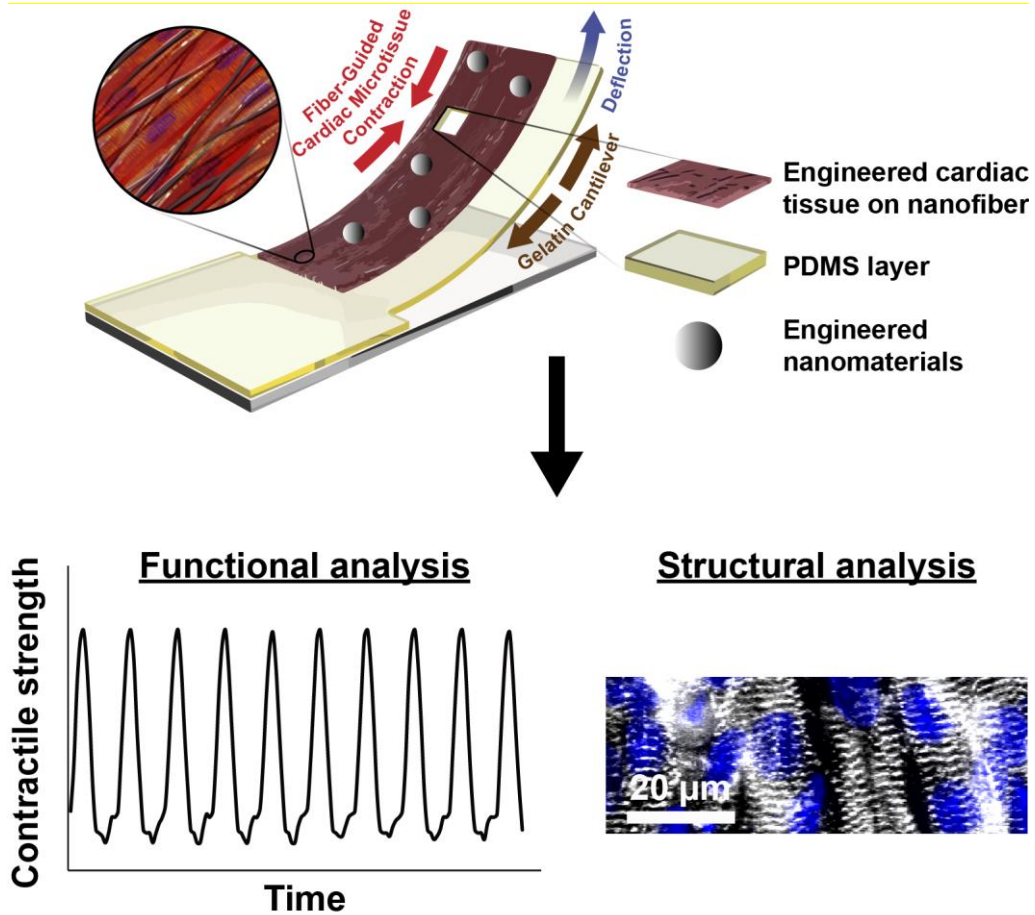


Figure 6. Effect of ENMs on calcium transient and sarcomere structure. a–h) Confocal images of calcium dye fluorescent (green) with calcium transient at the specific points (white boxes) for (a–b) control, (c–d) TiO_2 (10 $\mu\text{g/ml}$) exposure, and (e–f) TiO_2 (100 $\mu\text{g/ml}$) exposure. Scales are 500 μm . g–i) Confocal image of cardiomyocytes on nanofiber, stained for nuclei (blue) and α -actinin (grey). Scales are 100 μm (for the top panels) and 20 μm (for the bottom panels). The bottom panels are the zoom-in images from the red dots of the top panels. j) Orientational order parameter (OOP) analysis of cardiomyocytes after TiO_2 exposure. For statistical comparison with respect to control, ** $p < 0.05$, $n = 7$ for control (0 $\mu\text{g/ml}$) and TiO_2 (100 $\mu\text{g/ml}$) and 6 for TiO_2 (10 $\mu\text{g/ml}$).

1
2
3
4
5
6
7
8
9
10
11
12
13
14
15

1 **Graphical Abstract**

2

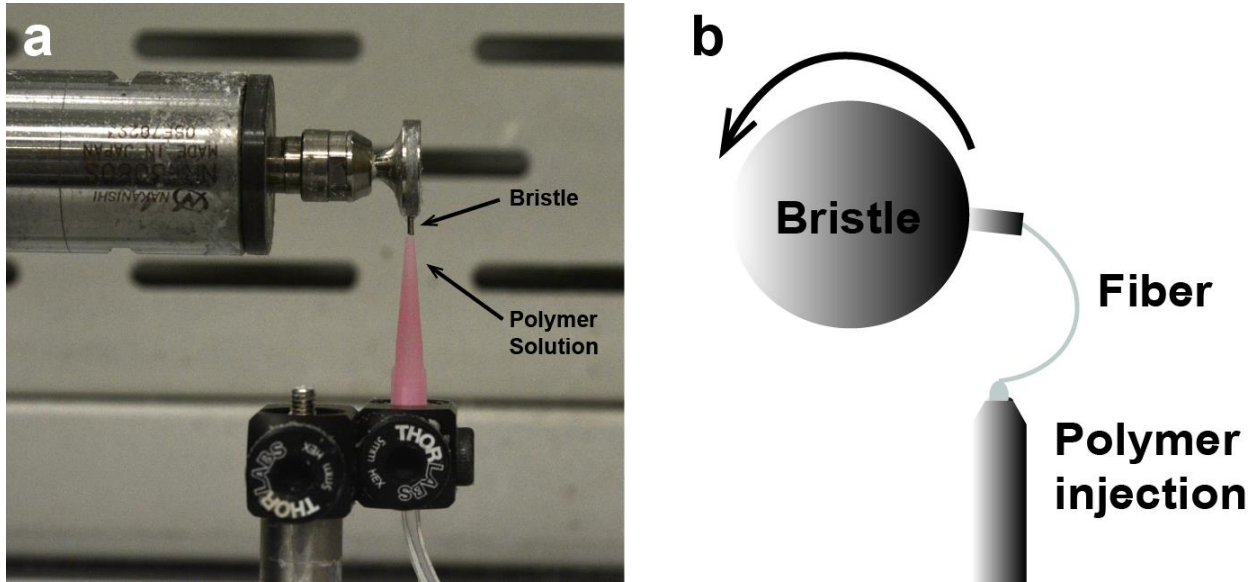


3
4
5
6
7
8
9
10
11
12
13
14
15
16
17
18
19
20
21
22

Mussel-inspired fiber scaffolds can be integrated with microphysiological systems for a high throughput assessment of contractile stress and structural defects for cardiac thin-films that are exposed to engineered nanomaterials.

1 **Supporting Information**

2



3

4 **Figure S1.** Image illustrating the pull spinning system used for nanofiber fabrication.

5

6

7

8

9

10

11

12

13

14

15

16

17

18

19

20

21

22

23

24

25

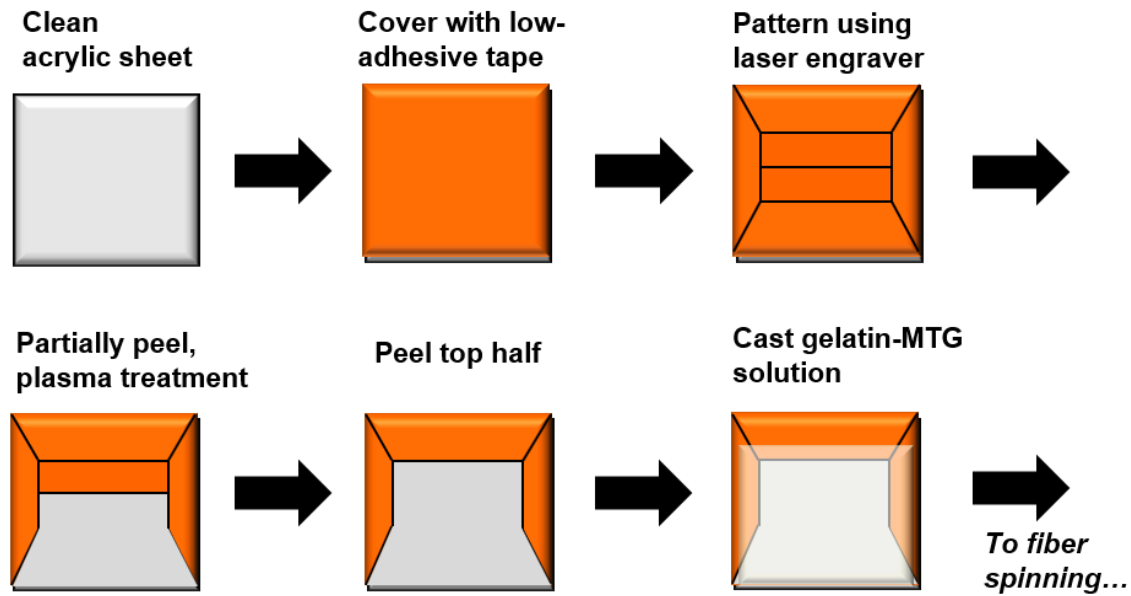
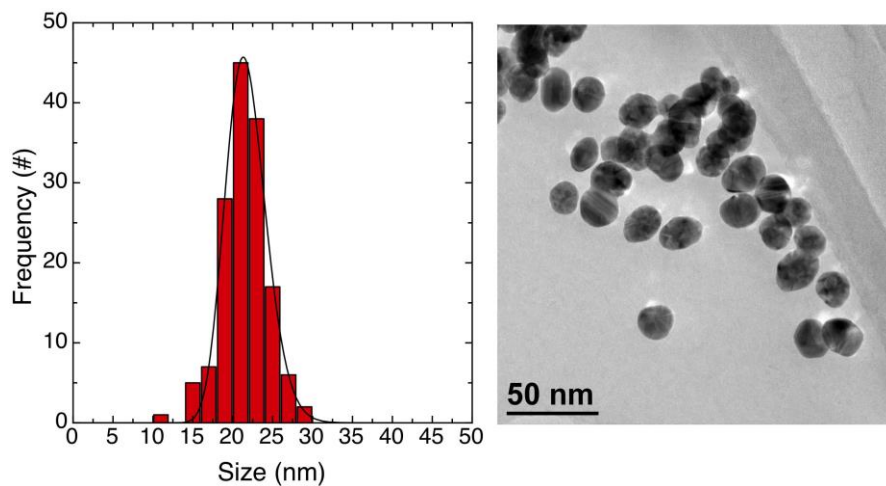
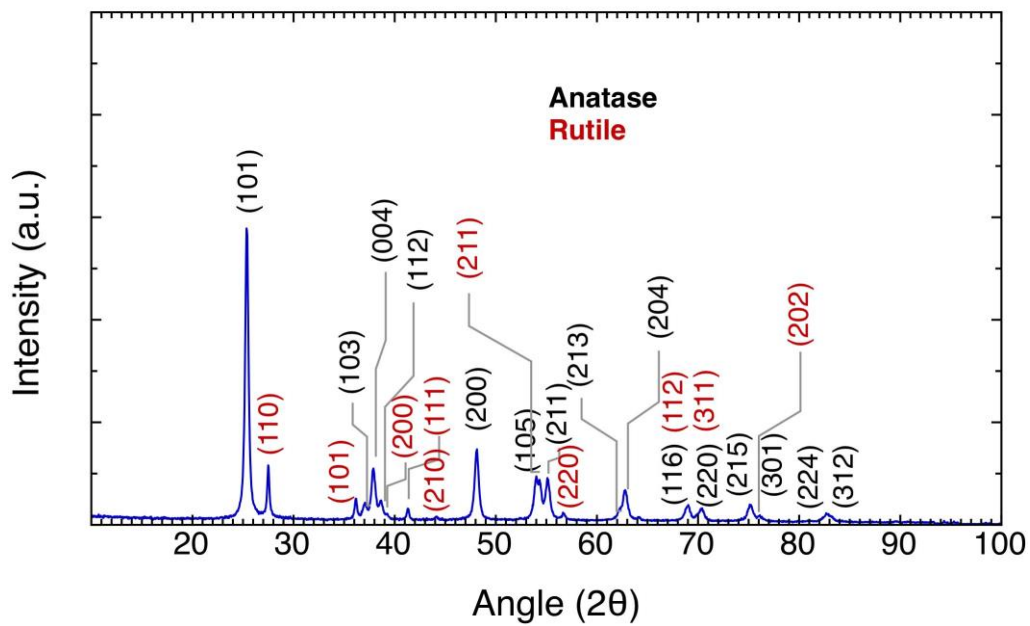


Figure S2. Schematic diagram showing the preparation of gelatin MPS substrates before spinning the fibers.

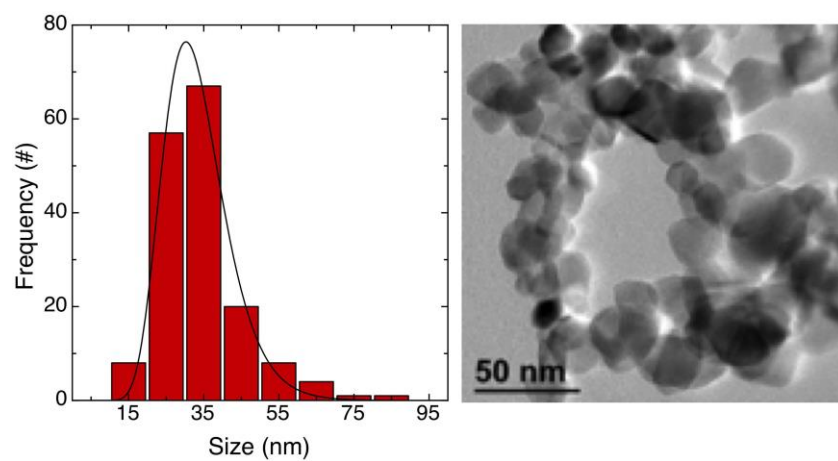
1
2
3
4
5
6
7
8
9
10
11
12
13
14
15
16
17
18
19
20
21
22



1
2 **Figure S3.** TEM Feret size distribution for the Ag nanoparticles.
3
4
5
6
7
8
9
10
11
12
13
14
15
16
17
18
19
20
21
22
23
24
25
26
27
28
29
30
31

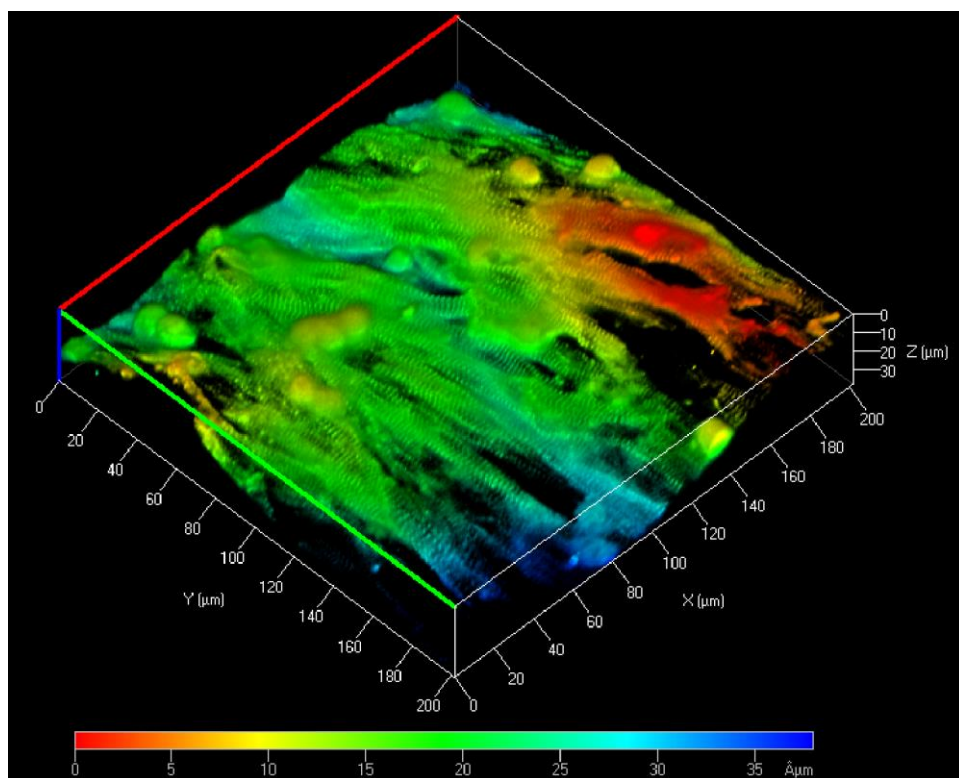


1
2
3 **Figure S4.** XRD Pattern for the TiO₂ Degussa P25.
4
5
6
7
8
9
10
11
12
13
14
15
16
17
18
19



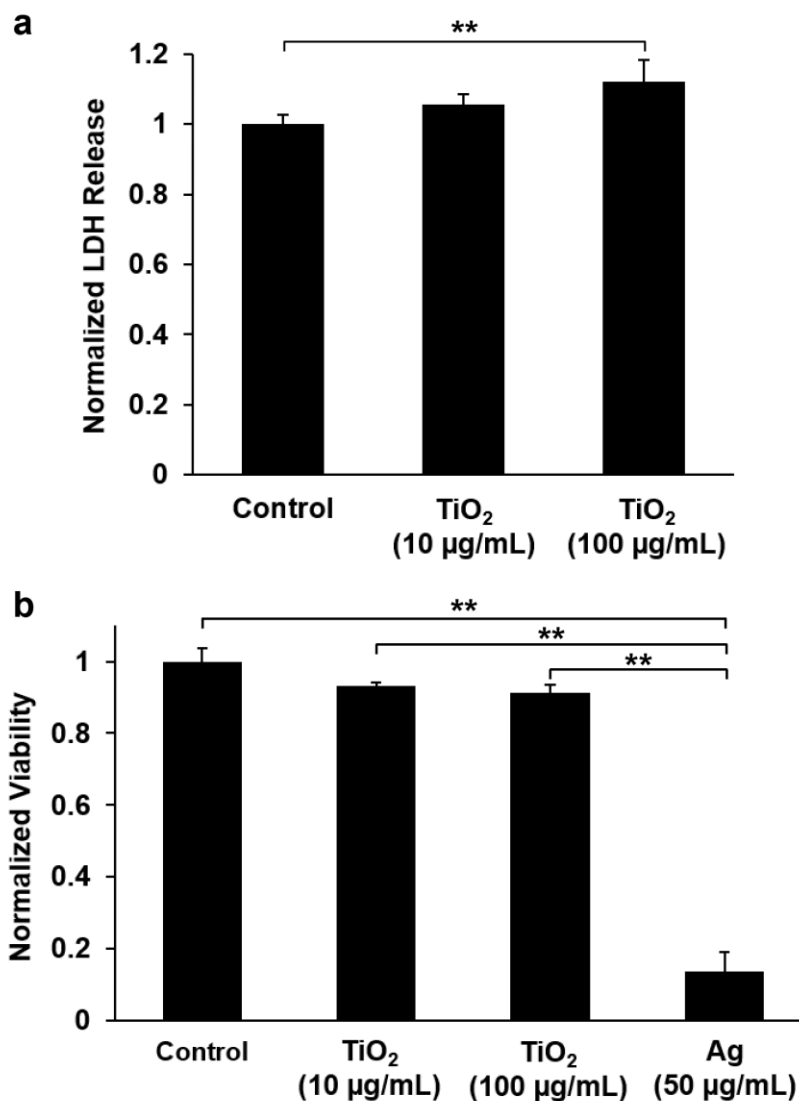
1
2
3 **Figure S5.** TEM Feret size distribution for the TiO₂ Degussa P25.
4
5
6
7
8
9
10
11
12
13
14
15
16
17
18
19
20
21
22
23
24
25
26
27
28
29
30
31
32

1



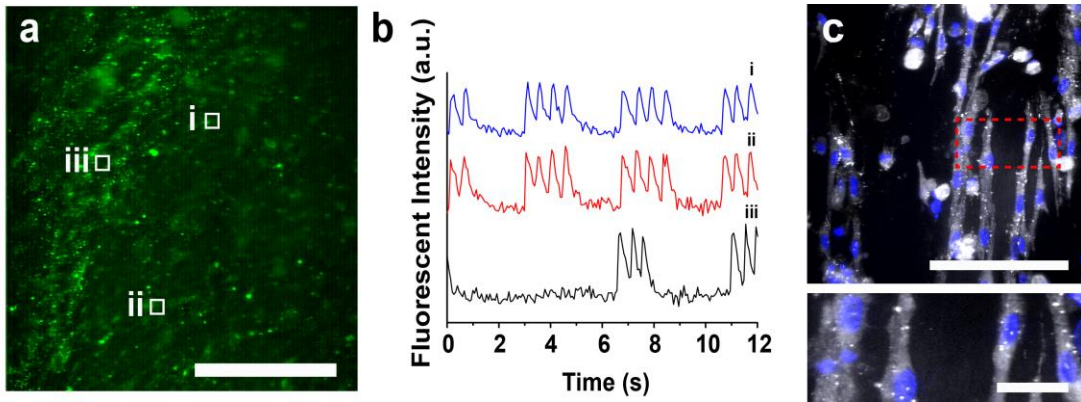
2

3 **Figure S6.** Representative 3D reconstruction image of z-stacked confocal images of NRVMs
4 grown on PCL/PDA nanofiber scaffold with a color depth.



1
2 **Figure S7.** Cytotoxicity tests for cardiomyocytes cultured on fiber MTFs. a) Comparison of
3 lactate dehydrogenase (LDH) release of cardiomyocyte MTFs, pre- and post-exposure to TiO₂ at
4 10 and 100 µg/mL. b) Comparison of cell viability based on MTT assay for cardiomyocytes
5 unexposed and exposed to 50 µg/mL Ag nanoparticles. Bars represent standard error, $n=8$ per
6 condition for LDH assay, $n=16$ for MTT assay. For statistical comparison, $**p<0.05$.

7
8
9
10
11
12
13
14
15



1
2 **Figure S8.** Effect of silver nanoparticle exposure. a–b) Confocal images of calcium dye
3 fluorescent (green) with calcium transient at the specific points (white boxes) for Ag (50 μ g/ml)
4 exposure. Scale is 500 μ m. c) Confocal image of cardiomyocytes on nanofiber, stained for nuclei
5 (blue) and α -actinin (grey). Scales are 100 μ m (for the top panels) and 20 μ m (for the bottom
6 panels). The bottom panels are the zoom-in images from the red dots of the top panels.
7
8
9
10
11
12
13
14
15
16
17
18
19
20
21
22
23
24
25
26

1 **Table S1.** Morphological and structural properties of ENMs

ENM	Primary Particle Size			Crystal Structure		
	SSA (m ² /g)	d _{BET} (nm)	d _{TEM} (nm)	d _{XRD} (nm)	Crystal System	Crystallinity (%)
TiO ₂ P25	46.45 ± 2.32	29.76 ± 1.49	28.82 ± 11.07	Anatase: 21.3 Rutile: 30.40	Anatase 81.4% Rutile 16.2%	81.4
Ag – citrate capped	N/A	N/A	21.58 ± 2.83	N/A	N/A	N/A

2 ENM, engineered nanomaterial; SSA by nitrogen adsorption/Brunauer-Emmett-Teller (BET)
3 method; d_{BET}, d_{TEM} and d_{XRD}, particle

4
5
6
7
8
9
10
11
12
13
14
15
16
17
18
19
20
21
22
23
24
25
26
27
28
29
30
31
32
33
34
35

1 **Table S2.** Physical properties of ENMs

ENM	Shape Factors			Porosity		ρ_{raw} (g/cc)
	Aspect ratio	Circularity	Roundness	TPV (cc/g)	APS [§] (nm)	
TiO ₂ P25	1.276 ± 0.162	0.926 ± 0.034	0.795 ± 0.094	0.119	5.14	4.38±0.01
Ag – citrate capped	1.175 ± 0.111	0.999 ± 0.025	0.858 ± 0.078	N/A	N/A	N/A

2 ENM, engineered nanomaterial; TPV and APS, total pore volume and average pore size,
3 respectively determined by nitrogen adsorption/Brunauer-Emmett-Teller (BET) method; ρ_{raw} , the
4 raw density of ENMs determined by nitrogen volume displacement (pycnometry); [§]TEM did not
5 confirm the presence of pores but interparticle spacing instead.
6

7

8

9

10

11

12

13

14

15

16

17

18

19

20

21

1 **Table S3.** Chemical and biological properties of ENMs

ENM	Chemical Elemental Composition				Recombinant Factor C (EU/mg) [‡]	Sterility (bacterial growth observed) [†]
	Trace Metal Analysis (%)	Carbon Content (%) [*]	Stoichiometry XPS	Stoichiometry ICP-MS		
TiO ₂ P25	99.98±4.86 Ti	0.22±0.13	TiO _{1.93}	TiO _{1.86}	< LOD	No growth
Ag – citrate capped	99.69±0.60 Ag	0.17±0.21	N/A	N/A	4.870	No growth

2 ENM, engineered nanomaterial; LOD, limit of detection; ^{*}Elemental plus organic carbon content
3 (w/w); [‡]Suspension tested at 10 µg/ml, endotoxins in PBS is 76 EU/ml; [†]suspension tested at
4 50µg/ml;

5
6
7
8
9
10
11
12
13
14
15
16
17
18
19
20
21
22
23
24
25
26
27
28
29
30
31
32
33
34
35

1 **Table S4.** Percentage of cantilevers beating during the time point of MPS optical recording.

Condition	% Cantilevers Beating
Control (0 $\mu\text{g/mL}$)	95.0%
TiO ₂ (10 $\mu\text{g/mL}$)	91.7%
TiO ₂ (100 $\mu\text{g/mL}$)	55.6%
Ag (50 $\mu\text{g/mL}$)	28.6%

2
3
4
5
6
7
8
9
10
11
12
13
14
15
16
17
18
19
20
21
22
23
24
25
26
27
28

1 **Supplementary Movies**

2

3 **Movie 1.** NRVM contraction on PCL/PDA nanofiber scaffolds. Scale is 100 μm .

4

5 **Movie 2.** NRVM contraction on fiber-coated gelatin MPS. Scale is 2 mm.

6

7 **Movie 3.** NRVM contraction on fiber-coated cardiac microphysiological device with embedded
8 contractility sensors.

9

10 **Movie 4.** Time-series images of a calcium-sensitive dye from cardiomyocytes grown on the
11 fiber-coated MTF sample without nanoparticle exposure.

12

13 **Movie 5.** Time-series images of a calcium-sensitive dye from cardiomyocytes grown on the
14 fiber-coated MTF sample with a low-dose TiO_2 (10 $\mu\text{g}/\text{ml}$) nanoparticle exposure.

15

16 **Movie 6.** Time-series images of a calcium-sensitive dye from cardiomyocytes grown on the
17 fiber-coated MTF sample with a high-dose TiO_2 (100 $\mu\text{g}/\text{ml}$) nanoparticle exposure.